Ground and excited states of bis-4-methoxybenzyl diketopyrrolopyrroles

Alanna S. Murphy,[a,b] Catherine E. Killalea,[a,b] Joshua Humphreys,[a,b] Paul A. Hume, [a,b]§ Matthew J. Cliffe,[b] Glen J. Murray,[b] E. Stephen Davies,[b] William Lewis[b]¶ and David B. Amabilino*[a,b]

[a] A.S. Murphy, C.E. Killalea, Dr. J. Humphreys, Dr. P.A. Hume and Prof. D.B. Amabilino

GSK Carbon Neutral Laboratories for Sustainable Chemistry

University of Nottingham

Triumph Road, Nottingham, NG7 2TU, UK

E-mail: david.amabilino@nottingham.ac.uk

[b] Dr. M.J. Cliffe, Dr. E.S. Davies, Dr. W. Lewis

School of Chemistry

University of Nottingham

University Park, Nottingham, NG7 2RD, UK

§ Dr. P.A. Hume present address

MacDiarmid Institute for Advanced Materials and Nanotechnology and School of Chemical and Physical Sciences

Victoria University of Wellington, Wellington 6010, New Zealand

¶ Dr. W. Lewis present address

Chemistry Building

The University of Sydney, Eastern Avenue NSW 2006, Australia

Abstract: A series of symmetrically bis-4-methoxybenzyl (4MB) N-substituted 1,4-diketopyrrolo[3,4-c]pyrrole (DPP) derivatives have been synthesized. The 4MB unit makes soluble DPPs, and shows noteworthy modification of ground and excited states of the core when compared with related alkyl derivatives. Absorption and emission spectroscopy, as well as electrochemical and computational methods have been employed to prove the importance of the peripheral aryl unitson the donor/ acceptor properties of the molecules. The 4MB products are highly fluorescent (quantum yields approaching 100% in solution), with unique distribution of frontier states shown in the spectroelectrochemistry. The frontier energy levels shows that this subtle substitutional change could be of future use in molecular energy level tailoring in these, and related, materials for organic (opto)electronics.

Introduction

Diketopyrrolopyrrole (DPP) based compounds have emerged rapidly as interesting molecules and materials for applications ranging from fluorescent probes[1-4] to optoelectronic devices.[5-10] The interest is stoked by their synthetic possibilities and their high thermal and photo-stability.[11] The planar core of these compounds (Figure 1) consists of a π-conjugated dilactam system which can be substituted with different aromatic groups at the 3- and 6-positions, and with alkyl derivatives as the N-substituents.[12,13] Thus, the compounds present a multitude of opportunities for structural and electronic modification via synthetic functionalization, such as end capping of the aromatic sections,[14,15] the addition of conjugated flanking units to extend charge delocalization[16,17] and solubilizing chains of varying polarity at the N position to aid processing.[18] This alkylation of DPP derivatives gives rise to solubility in relatively low polarity organic solvents,[19-21] as well as solubility in more polar solvents when heteroatom-containing chains are appended.[22,23] Appropriate substitution can modulate both intra-and inter-molecular interactions in the solid state.[21, 24]

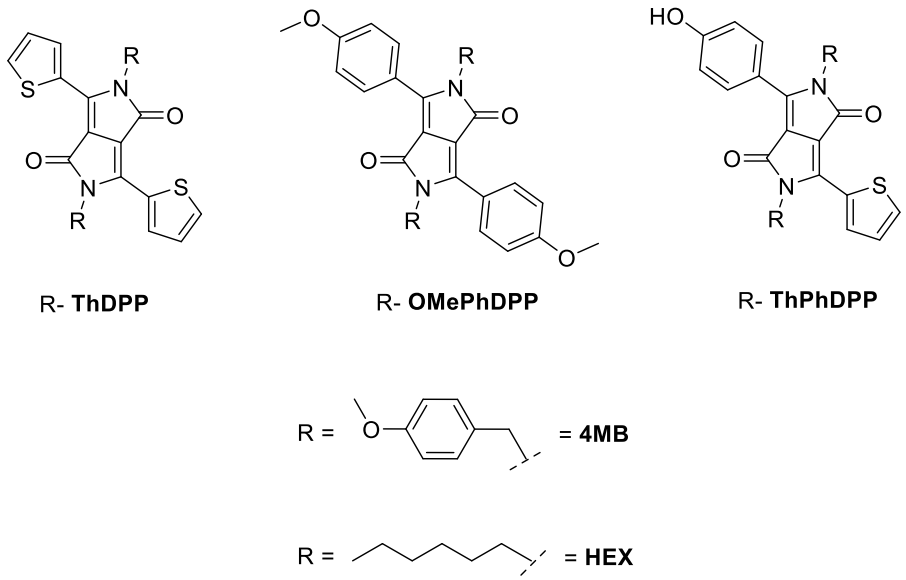

Figure 1. Structures and notation used for the DPP compounds synthesised and investigated. The common DPP core is indicated.

The ability to change and embellish the core DPP structure provides not only the opportunity to move towards donor- acceptor-donor type systems, which require fine tuning of the HOMO/LUMO energy levels,[25] but it also gives control over light absorption,[26] electrical transport[27] and crystallinity.[25] These properties are important features of the molecules as functional materials, especially in the field of optoelectronics. A more complete understanding how these properties are affected by structural modifications to the DPP core, in both the solid and solution phase will guide designs for more effective materials. Herein we report structural, spectroscopic and electrochemical properties of 4-methoxybenzyl (4MB) derivatives and we compare these properties with those of analogous compounds with an n-hexyl chain (Figure 1).

The electronic absorption profile of DPP derivatives have been explored thoroughly through experiment and theory, providing insight into the origin of the main absorption bands.[25] A dual band absorption structure is generally seen in donor-acceptor type

molecules and especially DPP systems which are known for having a donor- acceptor-donor nature.[11,25] The main, low energy absorption bands are related to intramolecular charge transfer occurring between the accepting core and the donating flanking units and in specific cases the vibronic structure of this band can be altered or broadened depending on the planarity of the molecule.

High fluorescence quantum yields are typical for DPPs in solution; the thiophene based DPPs have quantum yields over 70% (79% for n-hexyl [25] and 73% for a branched alkyl chain[28]). Phenyl DPP derivativesexhibit a range of quantum yields[29,30] that can be very high, depending on substituents and medium.[31,32] Recent work into the solid state structure of thiophene DPP highlights the difference in the packing arrangements adopted by mono and di-alkylated derivatives and the profound effect this can have on the absorption profile of the compounds. Furthermore, it shows the effect of the steric bulk of the alkyl chain in influencing the extent of twisting between the flanking thiophene units and the central core.[33] This comparative study shows that the extent of twisting between flanking phenyl units and the DPP core is associated with the steric repulsion between hydrogen atoms on the phenyl ring and those on the alkyl chain.

In the present work, we show a full spectroelectrochemical analysis of DPPs that reveals the charge distribution in the reduced and oxidized states. In addition, we show the interesting structural and optical features that arise from substitution with the 4MB derivatives.

Results and Discussion

Synthesis and characterization

Synthesis of the parent DPPs was carried out according to literature procedures[34-36] and N-alkylation of these compounds was carried out using standard[37] or more efficient[38] conditions giving the target compounds in moderate yields (similar to related compounds of this type) after purification (55% 4MB ThDPP, 57% 4MB OMePhDPP, 40% 4MB ThPhDPP). This structural modification facilitates solubility of the DPPs in common organic solvents, allowing for detailed structural and electronic characterization (see Supporting Information). The NMR, mass spectrometric and IR analysis all prove the identity of the compounds. The in depth opto-electronic characterization is described in the following sections.

Cyclic voltammetry and spectroelectrochemistry

The electrochemical behavior of DPP derivatives in general is largely understood, it commonly comprises two oxidation processes and a single reduction process.[25] The features seen in the new compounds are largely similar to those observed in N-alkyl DPPs (where a second irreversible reduction was seen at very negative potentials).[39-41] The oxidation processes are attributed to the comparatively electron rich flanking units and the single reduction arises from the electron accepting core. The combined cyclic voltammograms for the 4MB type compounds (Figure 2) show these traits, imparted by the 4MB group. Two oxidation processes are observed for 4MB ThDPP (scan rate dependence measurements can be found in the Supporting Information) at E1/2 0.58 and Epa 0.85 V and one reduction process at E1/2 –1.58 V (all relative to the ferrocenium-ferrocene couple used as an internal reference). It is noted that the ratio of currents in the forward and reverse directions for the first oxidation and the reduction

processes vary with scan rate; at lower scan rates the ratio of the return current is reduced suggesting an instability of the electrogenerated species at the electrode/diffusion layer.

Compound 4MB OMePhDPP has two oxidation processes at E1/2 0.58 V and E1/2 0.84 V, and a single reduction process at E1/2 -1.76 V. The first oxidation and reduction show consistent ratios of currents in the forward and reverse directions across the scan rates employed (see Supporting Information Figures SI3 and SI4), suggesting that methoxyphenyl flanking groups provide better stability for the electrogenerated species than the corresponding thiophene. The more negative potential of reduction for this compound indicates that the methoxyphenyl units are providing more electron density to the DPP central core than the corresponding thiophene units in 4MB ThPhDPP. As a result of the poor solubility in dichloromethane/electrolyte the cyclic voltammetry of 4MB ThPhDPP was performed in DMF. Noting this difference 4MB ThPhDPP, containing a both 4-hydroxyphenyl and thiophenyl flanking units, has a reduction process, at E1/2 -1.64 V, that occurs at a potential between those of 4MB ThDPP and 4MB OMePhDPP, showing again[13] that tuning of the frontier orbitals of the DPP core by the flanking groups is achieved readily. Compound 4MB ThPhDPP has an irreversible oxidation process at Epa 0.39 V and a further oxidation process at higher potential (see Supporting Information). Unlike 4MB ThDPP and 4MB OMePhDPP, the first oxidation of 4MB ThPhDPP shows no evidence for a reverse wave in the cyclic voltammetry at any of the scan rates reported. We suggest that this phenomenon may result of either the imposed choice of solvent (see above) or/and the instability of the oxidized species. For the reduction the ratio of currents in the forward and reverse directions vary with scan rate suggesting an instability of the electrogenerated species at the electrode/diffusion layer and this may relate to the presence of the thiophenyl unit.

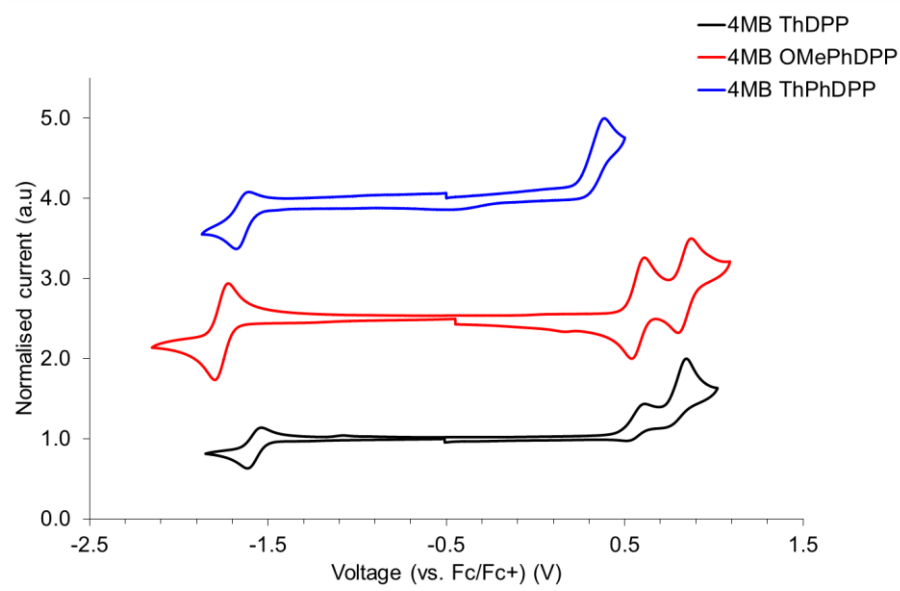

Figure 2. Cyclic voltammograms for the studied 4MB type compounds, obtained at scan rate = 0.10 V s-1, under an Ar atmosphere. Potentials are plotted against the ferrocenium/ferrocene couple used as the internal standard. In dichloromethane containing [n-Bu4N][PF6] (0.2 M) for 4MB ThDPP and 4MB OMePhDPP and DMF containing [n-Bu4N][PF6] (0.2 M) for 4MB ThPhDPP.

The highest occupied molecular orbital (HOMO) and lowest unoccupied molecular orbitals (LUMO) have been determined experimentally from electrochemical experiments where the HOMO and LUMO are calculated from the onset of the first oxidation and reduction waves, respectively. Table 1, shows the HOMO and LUMO energy levels of the studied compounds and using these values and comparisons are made to the hexyl derivatives. The computationally calculated energy levels are also shown in Table 1 and Figure 3 shows a visual representation of the electron distribution of the HOMO and LUMO across the molecule. Qualitative analysis of the data shows that the HOMO resides generally on the central core of the DPP, whereas the LUMO is more delocalised across the core (as for the lactam free compounds[42]) and the flanking units. There is very little contribution to either LUMO or HOMO from the 4MB group . The characteristics of the DPP derivatives are presumably dominated by the push-pull nature of the compound, as the HOMO, LUMO and gap values are essentially the same regardless of the N-substituent. The largest effect of the 4MB substituent is seen for the ThDPP core, where the gap is reduced when compared with the hexyl group, as a result of raising of the HOMO and lowering of the LUMO.

Table 1. Experimentally and computationally determined HOMO and LUMO energy levels of the studied compounds. Where the experimental values have been calculated from the cyclic voltammograms using the equations: E(HOMO)= -E[EOXonset + 4.8], E(LUMO)= -E[EREDonset + 4.8]. Theoretical values have been obtained using TD-DFT with a B3LYP[43-45] hybrid functional and a 6-31G (d) basis set.

Compound	**$HOMO_{expt}$ (eV)**	**$LUMO_{expt}$ (eV)**	**$E_{g,\ expt}$ (eV)**	**$HOMO_{calc}$ (eV)**	**$LUMO_{calc}$ (eV)**	**$E_{g,\ calc}$ (eV)**
4MB ThDPP	-5.33	-3.30	2.03	-5.02	-2.40	2.62
HEX ThDPP[10]	-5.56	-3.10	2.46	-4.91	-2.47	2.44
4MB OMePhDPP	-5.30	-3.12	2.18	-4.82	-2.10	2.72
HEX OMePhDPP	-5.25	-3.11	2.14	-4.81	-2.11	2.70
4MB ThPhDPP	-5.05	-3.22	1.83	-4.99	-2.28	2.71
HEX ThPhDPP	-5.03	-3.20	1.83	-4.93	-2.27	2.66

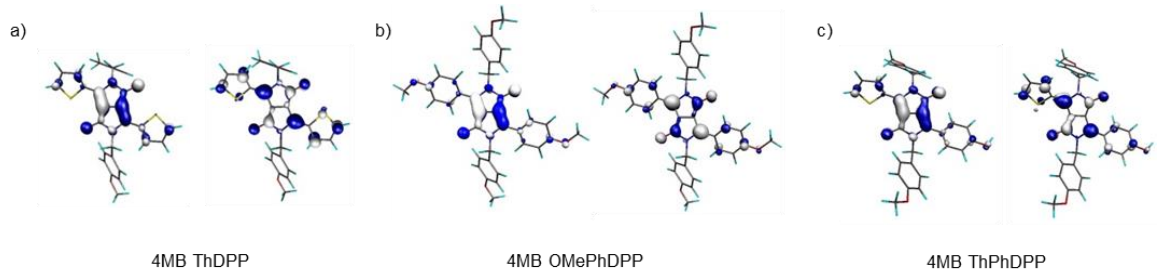

Figure 3. Computationally calculated HOMO (left) and LUMO(right) molecular orbitals for a) 4MB ThDPP, b) 4MB OMePhDPP and c) 4MB ThPhDPP. Simulated using Molekel from DFT calculations using Gaussian.[46]

An energy level diagram for the 4MB derivatives is plotted in Figure 4 to summarize the data. The equivalent hexyl species are included for comparison along with two classic donor and acceptor materials, P3HT and PC60BM. The plot shows that the DPP derivatives are largely donating in nature with the thiophene derivatives generally having more low-lying HOMO levels, in comparison to the mixed derivatives. The experimental and theoretical HOMO energy levels are in good agreement however the LUMO levels do not correlate and are overestimated by 0.3 – 1.0 eV (in DFT Koopman's theorem does not apply to the LUMO so this is a commonly observed glitch[47,48] which suggests that DFT employed here is reliable for comparative purposes, if not quantitative).

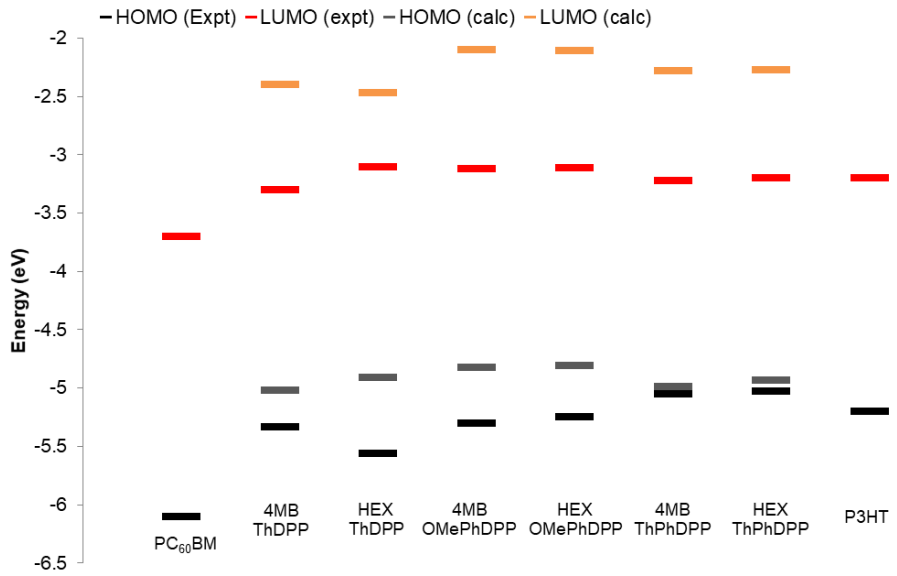

Figure 4. Comparison of the experimental and theoretically determined HOMO and LUMO energy levels for the compounds studied.

The spectroelectrochemistry of DPP compounds has been only scarcely explored to our knowledge.[49,50] Therefore there is a need to study this aspect of the materials and gain understanding of the electronic and absorption properties of the radical species produced by oxidation and reduction of this family of compounds. The UV-visible spectroelectrochemical data for the first oxidation and first reduction of 4MB ThDPP is shown in Figure 5. Oxidation of neutral 4MB ThDPP at 273 K results in significant changes to the absorption spectrum. Specific redox inter-conversion of the neutral form to a new species is indicated by the isosbestic points and the generation of a series of new broader, lower energy absorption bands. We infer from the observation of isosbestic points that, under the conditions of the experiment, the redox process proceeds in the absence of long-lived intermediates or transition states. Upon oxidation, the main absorption peak at 560 nm is depleted and this loss of intensity is accompanied by the generation of two intense, low energy absorption bands at 616 nm and 860 nm, along with two weak bands at 764 nm and 796 nm, the interconversion progressing smoothly through an isosbestic point. In the UV region, depletion of the (π-π*) band at 290 nm is accompanied by generation of a structured lower energy band at 345 nm, with this interconversion progressing through an isosbestic point at 301 nm. Reduction of the oxidized solution regenerated the spectral profile of the neutral species, albeit with some intensity loss in the main visible bands (Supporting Information Figure SI7) indicating limited decomposition over the long timescale of the experiment (ca. 1-2 hours).

The absorption spectrum of the singly reduced species of 4MB ThDPP generated by in-situ reduction of the neutral species shows loss of the visible bands and formation of a sharp intense band at 630 nm and a weak band at 825 nm for the anion. The inter-conversion is evidenced by an isosbestic point at 560 nm. In the UV region reduction resulted in general depletion of bands. Attempts to regenerate the neutral species by oxidation of the anion gave the correct spectral profile albeit with intensity loss across the spectral range (Supporting Information Figure SI8) indicating that the reduced species is susceptible to some decomposition over these longer experimental timescales, a conclusion similar to that made for the oxidized species.

The UV/vis spectroscopic data for the oxidation of 4MB OMePhDPP, at 273 K, is shown in Figure 6. Oxidation results in a general red shift of spectral features; the visible bands for 4MB OMePhDPP are depleted and new bands for the cation emerge, at 704 nm and 770 nm, the transformation proceeding through an isosbestic point at 531 nm. At higher energy the (π-π*) band for the neutral species, at 330 nm, is replaced with a new band at 368 nm for the cation passing through an isosbestic point at 344 nm. Reduction of the cation regenerates the spectral profile of the neutral species (Supporting Information Figure SI9) indicating that the oxidation process is essentially chemically reversible under these conditions. Reduction of 4MB OMePhDPP produces the spectral profile of the anion. Bands in the visible region arising from the neutral species are replaced by a strong absorption band at 600 nm corresponding to the anion, with the interconversion generating an isosbestic point at 530 nm (Figure 6). Additional bands are noted at lower energy and the spectral profile is broadly consistent with that of observed for 4MB ThDPP. Upon oxidation of the anion spectral features consistent with those of neutral 4MB OMePhDPP are regenerated although changes in relative intensities are noted (Supporting Information Figure SI10).

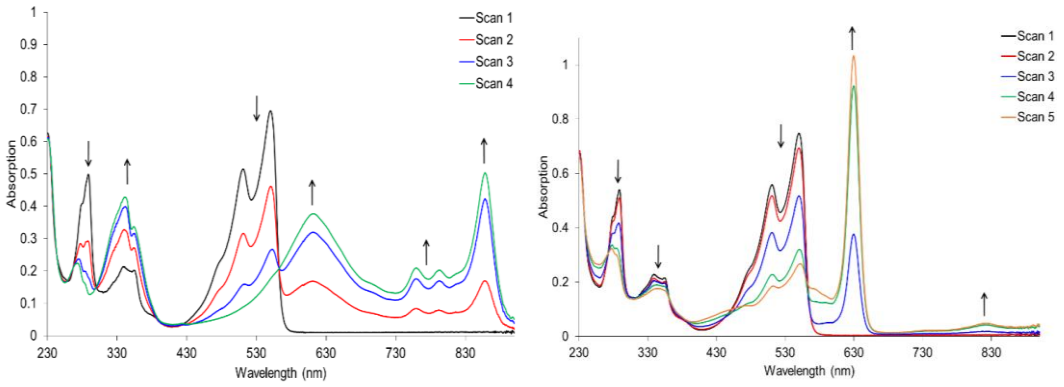

Figure 5. UV-visible absorption spectra of 4MB ThDPP showing the changes in the absorption profile as a result of oxidation (left) and reduction (right). In dichloromethane containing [n-Bu4N][PF6] (0.2 M) as the supporting electrolyte, at 273 K.

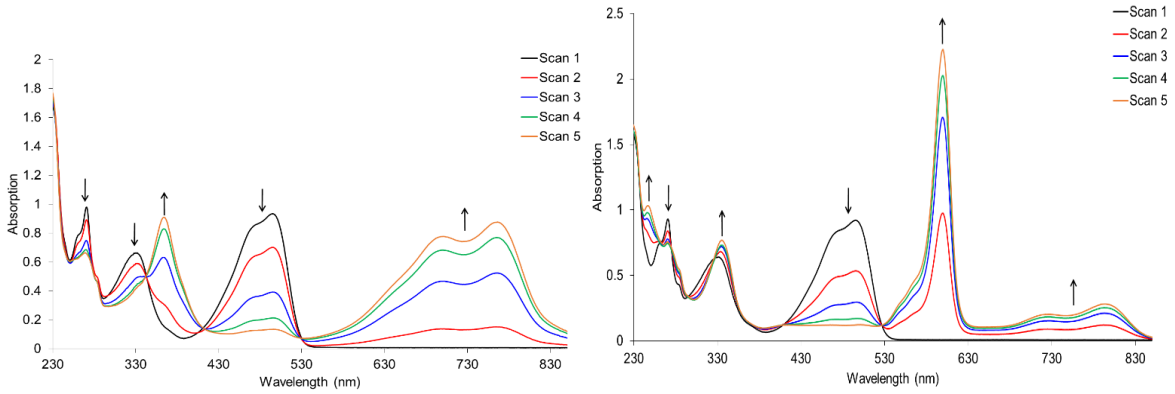

Figure 6. UV-visible absorption spectra of 4MB OMePhDPP showing the changes in the absorption profile as a result of oxidation (left) and reduction (right). In dichloromethane containing [n-Bu4N][PF6] (0.2 M) as the supporting electrolyte, at 273 K.

The UV-visible spectroelectrochemical behaviour for the reduction of 4MB ThPhDPP is shown in Figure 7. A band consistent with the formation of the anion, at 626 nm, is generated but variation of the spectral profile over time and the absence of clear isosbestic pointssuggests that the generated species was unstable under the conditions of the experiment (see above). Noting the results of the CV experiment, attempts at oxidation were not performed.

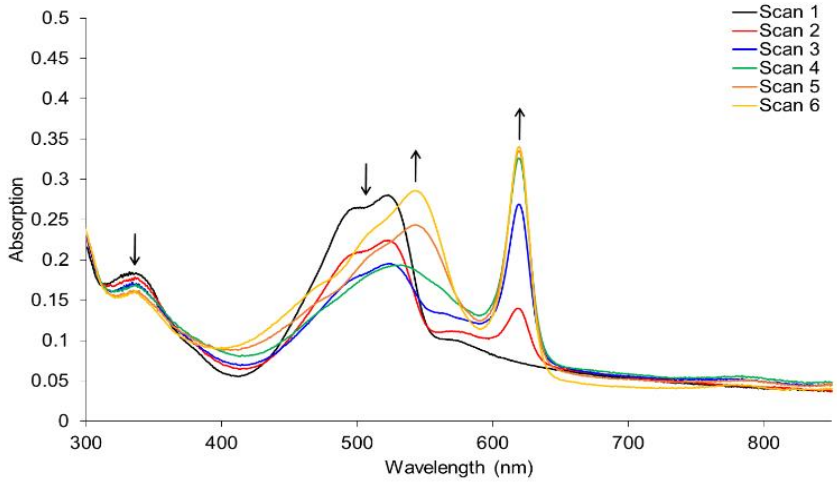

Figure 7. Spectroelectrochemical data for 4MB ThPhDPP upon reduction.). In DMF containing [n-Bu4N][PF6] (0.2 M) as the supporting electrolyte, at 273 K.

Solution phase absorption and emission spectroscopy

Absorption and emission spectra for the studied compounds in dichloromethane are shown in Figure 8, the spectra have been normalised in order to draw comparisons between the absorption and emission profiles and wavelengths for the compounds. It can be seen that all 4MB derivatives exhibit dual band absorption characteristics. All show a main absorption band occurring at approximately 500 nm attributed to the strong intramolecular interactions caused by the donor- acceptor- donor nature of the molecule, and a high energy band at approximately 330 nm indicative of the (π-π*) transition. Both thiophene-containing compounds exhibit vibronic structure within the low energy band with maxima occurring at 509 and 546 nm for 4MB ThDPP and 494 and 521 nm for 4MB ThPhDPP. It is known that in the phenyl DPP case, vibronic structure is broadened upon alkylation due to twisting occurring between the phenyl ring and the core of the molecule, resulting in loss of planarity and therefore vibronic information is not resolved.[51] This effect is clearly observed in the 4MB OMePhDPP case where the peak is broadened. It is also partially observed in the case of 4MB ThPhDPP which is expected to have a large degree of twisting between the phenyl ring and the core but not as much between the thiophene ring and the core. Loss of vibronic structure in the absorption spectrum of DPP type molecules is often related to the degree of twisting in the molecules as it is observed on going from an unalkylated to an alkylated DPP derivative,[47] although the resulting loss of rigidity is presumably responsible for the lack of vibronic bands seen in flat conjugated conformations. Upon alkylation, the molecule becomes twisted as a result of intramolecular steric interactions between the protons on the alkyl chain and the aryl flanking units, and presumably becomes more fluxional. This twisting reduces the extent of orbital overlap between the donor and acceptor units therefore destabilizing excited states within the molecule. A direct result of the lack of orbital overlap is a decrease in the molar extinction coefficients observed for these three varieties of molecules.

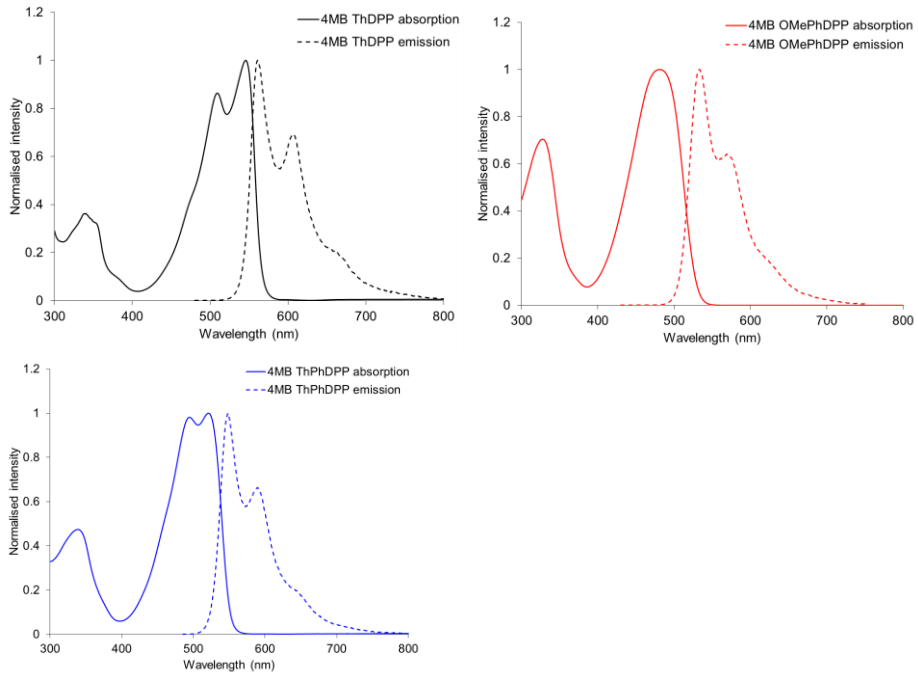

Figure 8. Absorption and emission spectra of the studied 4MB DPP derivatives in dichloromethane.

Table 2. Absorption and emission parameters for the studied compounds. Emission spectra were recorded at excitation wavelengths of 470 nm (ThDPP), 420 nm (OMePhDPP) and 475 nm (ThPhDPP) and referenced with Rhodamine 101.

Compound	Absorption λ_{max} (nm)	ε ($M^{-1}cm^{-1}$)	Emission λ_{max} (nm)	Stokes shift (nm)	φ (%)
4MB ThDPP	509, 546	39200	561, 608	15	89
HEX ThDPP[10]	510, 550	42400	562, 606	12	79
4MB OMePhDPP	481	23600	533, 573	52	>99
HEX OMePhDPP	478	26900	536, 567	58	90
4MB ThPhDPP	494, 521	26000	548, 590	27	83
HEX ThPhDPP	498, 520	26400	547, 582	27	40

Molar extinction coefficients for the maximum bands for each molecule are shown in Table 2. The molar extinction coefficient is lowest for the 4MB OMePhDPP case because of the twisting in the molecule, whereas the thiophene and mixed example have extinction coefficients which are higher. In these case, very little energy is lost to vibrational relaxation, which is further shown by the small Stokes shift of 15 nm observed. Compound 4MB ThDPP exhibits emission maxima at 561 nm with a smaller, lower energy band at 607 nm that is opposed to the absorption spectrum where the low energy band occurs at higher intensity. The shape of the emission spectra for the three compounds is similar therefore indicating that the emitting energy level is the same and presumably the conformation with greatest conjugation. The absorption and emission spectra for 4MB ThDPP show mirror image behaviour, which is expected. In contrast, the OMePhDPP derivative shows non mirror image spectra, where the emission maximum is at 561 nm, with a less intense and lower energy band at 607 nm. This again is attributed to the high degree of twisting present in the structure where the ground state and excited state are no longer similar in geometry so lower energy transitions are no longer resolved in the spectrum. The emission –parameters are shown in Table 2 with the spectra performed in the solution phase. From the data it is established that the DPP compounds with 4MB N-substituents have high quantum yield values when compared with the hexyl analogues, and approaching 100% in the best case. This is interesting as, generally, DPP derivatives have high quantum yield values (even in relatively twisted structures)[52] and we did not foresee that changing the alkyl chain would result in an increase in the value because they do not obviously participate in the frontier orbitals. However, in the cases reported here the quantum yield is at least 10% higher for the 4MB derivatives, and, perhaps most importantly, 40% higher for the thiophene derivative. From the simulations it is clear that the 4MB unit is not involved in the HOMO or LUMO levels of the DPP core, suggesting this effect is not electronic but more structural. There is essentially no difference between the absorption and emission wavelengths of 4MB and hexyl derivatives for any given compound, so conjugation is not affected greatly by changing the N-substituent. Therefore, we believe it arises from a restricted intramolecular rotation effect[53] whereby the 4MB group hinders free rotation of the aromatic groups more than the hexyl chainsThe potentially higher vibrational motion of the hexyl chain compared to the 4MB unit means that energy of the excited state can be lost through intramolecular rotation in the molecule resulting in decreased fluorescence quantum yield.[54,55] . It is noteworthy that aromatic N-substitution does give compounds with high quantum yields (around 80%, similar to the alkyl compounds), but in this case rigidity might accompany other effects that do not give rise

to the enhancement seen for the 4MB derivatives presented here.[56] Indeed, an N-hexyl morpholino pyridyl DPP derivative shows almost quantitative quantum yield.[57] Compared with a similar benzyl derivative,[58] 4MB OMePhDPP has higher quantum yield, suggesting that the 4MB group is perhaps unique in enhancing the fluorescence to such a degree. The exact reasons for these subtle changes are unclear at present, but the relative conformational rigidity of the 4MB group that has a specific orientation (see X-ray crystal structures below) may play a role.

Solid state structure, absorption and emission

The solid state absorption and emission spectra are shown in Figure 9. Logically, the spectra are all broader with respect to the solution phase spectra as a result of intermolecular interactions in the solid phase. The nature of these interactions determine the colour and intensity of fluorescence in DPPs.[59] The main point of interest in the compounds presented here is the shift in the spectra and the information this data provides about H- and J-type aggregation in the solid state. For 4MB ThDPP and 4MB OMePhDPP the solid state spectra are red shifted by 34 nm and 30 nm respectively, relative to the solution spectrum which is characteristic of J-type aggregation. Conversely the 4MB ThPhDPP derivative, is blue shifted by 17 nm showing H type aggregation in the solid phase. This feature was confirmed by analysis of crystallographic data.

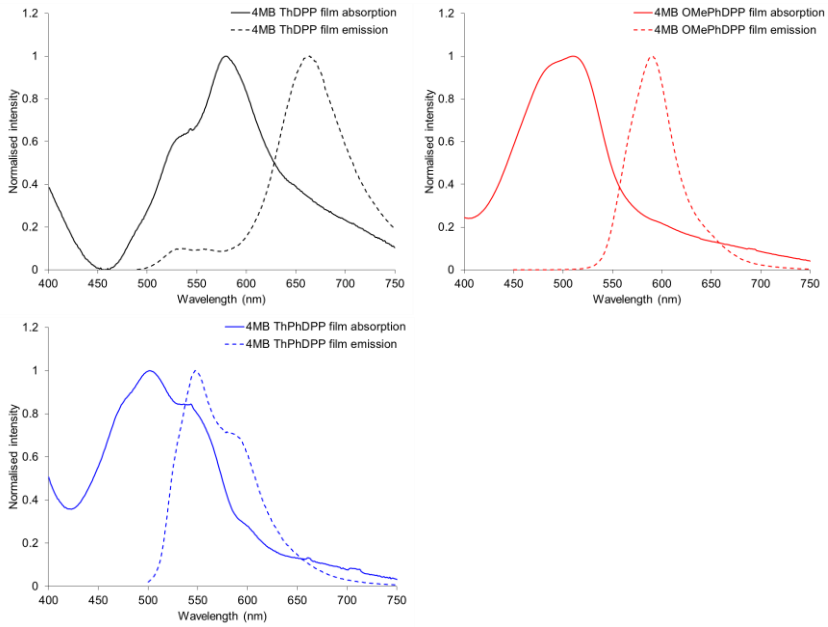

Figure 9. Solid state absorption and emission spectra of the 4MB DPP compounds. Emission spectra were recorded at excitation wavelengths of 470 nm (4MB ThDPP), 420 nm (4MB OMePhDPP) and 475 nm (4MB ThPhDPP).

Table 3. Absorption and emission parameters for the studied compounds.

Compound	Absorption λ_{max} (nm)	Emission λ_{max} (nm)	Stokes shift (nm)
4MB ThDPP	580	664	84
4MB OMePhDPP	511	592	81
4MB ThPhDPP	504, 537	548, 585	44

The solid state structure of the compounds was elucidated by single crystal X-ray diffraction. Plate and needle like crystals were obtained for 4MB ThDPP and OMePhDPP derivatives, respectively, by slow evaporation from dichloromethane. Plate crystals were obtained for the 4MB ThPhDPP derivative from slow evaporation of dimethylformamide.

The single crystal X-ray structures of the compounds are shown in Figure 10. In all molecules the 4MB group is quasi perpendicular to the DPP plane with dihedral angles of 85.8°, 89.5° and 88.7° for ThDPP, OMePhDPP and ThPhDPP respectively. This interesting conformational feature is also seen for benzyl derivatives,[14] and the methoxy substituent does not alter significantly the orientation of the group. In 4MB ThDPP the thiophene rings are arranged in the anti orientation with the sulphur atoms oriented towards the alkyl chain, which is similar to previously reported dialkyated compounds containing this core.[33] In the mixed derivative there is disorder between the phenol and thiophene flanking units; however, even in this case, the thiophene moiety is again oriented towards the substituent at the nitrogen atom. The packing arrangement of these materials is shown in Figure 10. The thiophene derivative has a classic herringbone arrangement. The packing of 4MB OMePhDPP shows a more-cross shaped structure which is thought to be the effect of the twisting of the flanking units of the plane of the core[60] combined with the steric bulk of the chain, thus creating a cross shaped molecule. This results in an unusual packing arrangement showing an edge to face type interaction of the alkoxyl phenyl unit with the flanking phenyl rings. The 4MB ThPhDPP structure shows the formation of stacked ribbons which is caused by hydrogen bonding between the phenol and the carbonyl moiety on the neighboring molecule and in this case the hydrogen bonded network extends to the supramolecular scale resulting in the packing arrangement shown in Figure 10. Various parameters have been extracted from the structural data and are shown in Table 4. It is possible that the bulkiness of the 4MB unit can drastically affect the extent of twisting within the molecule alongside other factors. In the OMePhDPP example, this large extent of twisting between the lactam core and the directly linked OMePh flanking units is a result of repulsive interactions between protons on the phenyl ring and those on the nitrogen substituent.[33] When we consider a smaller group such as the thiophene unit, this high torsion angle is not observed and planarity is attained. In the case of the mixed unit, the thiophene torsion angle is increased with respect to the symmetric thiophene based DPP and there is smaller twisting about the phenyl- DPP bond. The known inter-planar distance for ThDPP molecules with hexyl chains incorporated at the N positions is 3.614 Å,[61] and because of the larger steric bulk of the 4MB unit, larger intermolecular distances are observed for this family of compounds, of 3.981, 3.982 and 6.450 Å, respectively. 4MB ThDPP shows very large longitudinal displacement, where the thiophene, donating moiety residues directly above the accepting lactam ring (DPP core) of the neighboring molecule. This is indicative of J type aggregation[62] and is further supported by the bathochromic shift between the solution and solid absorption spectra.

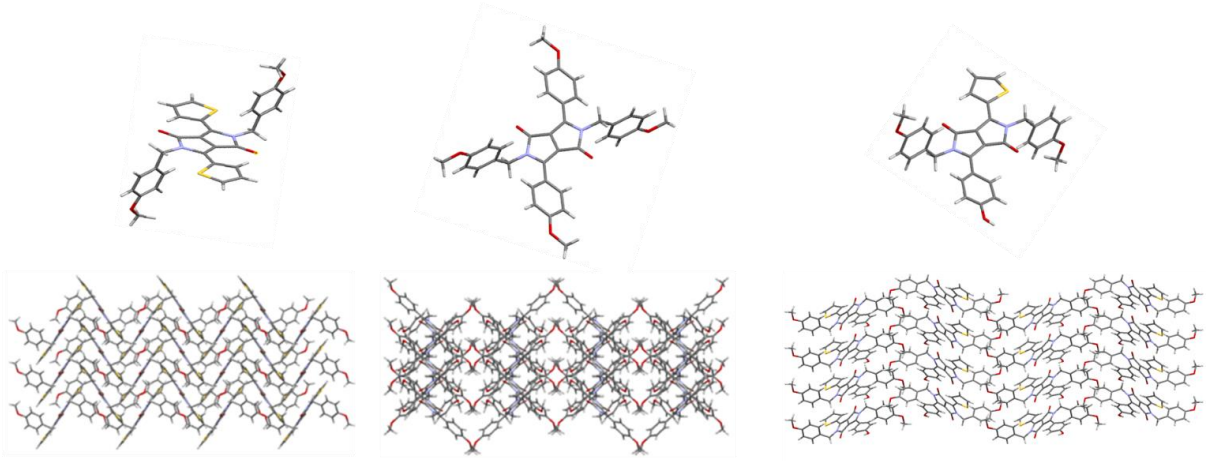

Figure 10. Single crystal X–ray structures of 4MB ThDPP, OMePhDPP and ThPhDPP respectively, showing the molecular conformation. (top) and packing arrangement (bottom)

Table 4. Measured values for interplanar distances between aryl-lactam centroids, displacement along the long, short and vertical axes. Also shown are the measured torsion angles between the DPP plane and the aryl unit and the out of plan angle between the DPP core and the 4MB unit.

Name	**Aryl-Lactam centroids (Å)**	**Inter-planar distance (Å)**	**Displacement (Å)**			**DPP-Aryl (°)**	**Lactam-[Clactam-N-C(R)] (°)**
			Long	Lat	Vert		
4MB ThDPP	3.98	3.56	5.04	1.48	3.61	9.44	13.01
4MB OMePhDPP	3.98	3.87	3.61	0.16	3.87	34.71	14.77
4MB ThPhDPP	6.45 (Th) 7.40 (Ph)	3.28	3.43 (Th) 4.91 (Ph)	5.22 (Th) 2.34 (Ph)	3.47 (Th) 3.25 (Ph)	14.27 (Th) 21.45 (Ph)	3.79

The OMePhDPP material shows the same effect as a result of the combination of large longitudinal displacement and short lateral displacement. In contrast, the compound incorporating phenyl and thiophene lateral units has much larger lateral displacement and small longitudinal displacement. Therefore, 4MB ThPhDPP shows a more overlapped face to face type stacking arrangement , leading to a quite short π-π inter-planar separation (3.28 Å). This feature explains the solid state absorption spectrum of this material. In addition, edge to face type interactions are observed between the thiophene and the methylene protons of the 4MB units on neighboring molecules, and there is large contribution to both lateral and longitudinal displacement, thus confirming contribution from both H and J type aggregation observed in the optical properties.

Conclusions

The 4MB substituent for the DPP chromophore shows some unique features compared with other compounds that has effects on both solution state optical properties as well as the structure and properties in the solid state. In solution, the high quantum yields might indicate the potential use of these molecules as highly efficient materials for sensing as fluorescent probes or in organic light emitting diodes. The high quantum yields would give good Förster resonance energy transfer rates which could auger well for use of related materials in photovoltaic devices.[63] The spectroelectrochemical study has shown the dramatic change in absorption of the compounds upon oxidation or reduction, and may indicate potential as electrochromic materials. The relative stability of the oxidised and reduced forms of two of the compounds is interesting for a number of opto-electronic device uses. The electrochemical measurements show how the 4MB unit modifies the HOMO-LUMO gap and energy levels, modulating the properties of the DPP core structure particularly in the case of the thiophenyl-containing compounds. This observation indicates that this kind of lateral unit can assist in fine–tuning their electronic properties to be matched with other donor/ acceptor materials in order to fulfil specific roles. The crystallographic study gives a good indication of how these derivatives may act when incorporated into organic solar cells, for example. Ideal donor-acceptor-donor stacks of planar molecules will aid charge transport and it has previously been found that that photovoltaic performance is enhanced as a result of J type aggregation.[64] While the methoxy substituent has been used on the flanking groups here, replacement of this unit with others is likely to provide materials with unique and useful characteristics.

Experimental Section

All commercially available reagents and solvents were used as received unless stated otherwise. Parent thiophene, 4-methoxyphenyl and thiophene-phenol diketopyrrolopyrrole compounds were synthesised according to published synthetic procedures[24-26] and N-alkylation was carried out according to literature.[27,28] Cyclic and square wave voltammetry experiments were carried out using an Autolab PGSTAT20 under an argon atmosphere using a three-electrode arrangement in a single compartment cell. A glassy carbon working electrode, a platinum wire secondary electrode and a saturated calomel reference electrode were used in the cell. The reference electrode was chemically isolated from the test solution using a bridge tube terminated with a Vycor frit and containing electrolyte solution. An analyte concentration of ca. 1.0 mM was used with [n-Bu4N][PF6] as a supporting electrolye in dichloromethane (0.2 M) for 4MB ThDPP and 4MB OMePhDPP. An analyte concentration of ca. 1.0 mM was used with [n-Bu4N][PF6] as a supporting electrolyte in dimethylformamide (0.1 M) for 4MB ThPhDPP owing to poor solubility in dichloromethane. Redox potentials are referenced to the ferrocenium/ferrocene couple used as the internal standard. No compensation was applied for internal resistance. UV-visible spectroelectrochemical measurements were performed in a PerkinElmer Lambda 16 spectrometer using an optically transparent electrochemical cell, consisting of a modified quartz cuvette with a 0.5 mm path length. A three-electrode configuration of a platinum/rhodium gauze working electrode, platinum wire secondary electrode and a saturated calomel reference electrode (chemically isolated as above) were used in the cell. The potential at the working electrode was controlled with a Sycopel Scientific Ltd DD10M potentiostat. Temperature control was achieved by passing a stream of chilled nitrogen across the surface of the cell. Solvents and electrolyte concentrations were identical to those reported for the compounds above. Absorption spectra were carried

out using UV/visible NIR Agilent CARY spectrometer. Solid film samples were prepared by drop casting from THF. Emission measurements were carried out using photoluminescence spectrometer FLS890. Fluorescence quantum yield values were carried out using photoluminescence spectrometer F980 and EMT integrating sphere. Samples were referenced against Rhodamine 101 (5.0E-6 M in EtOH). Crystals of 4MB ThDPP and 4MB OMePhDPP were mounted on MicroMounts (MiTeGen) using YR-1800 perfluoropolyether oil and cooled rapidly to 120 K in a stream of cold nitrogen using an Oxford Cryosystems open flow cryostat. X-ray diffraction was recorded on Rigaku Oxford Diffraction XtalLab Pro diffractometer, using Micromax 007 HF Copper Rotating Anode source collimated by a VariMax VHF mirror optic, equipped with Pilatus3 R 200K detector. 4MB ThPhDPP data was collected at Diamond Light Source beamline I19. In all cases, crystals were cooled with Oxford Cryosystems open flow cryostats. Data was collected with CrysAlis Pro and structures were solved with Olex2.solve, using SHELX for refinement and OLEX2 as an interface. Synthetic experimental details are given in the Supporting Information.

Acknowledgements

We thank the EPSRC (project EP/M005178/1), GlaxoSmithKline, and the School of Chemistry at the University of Nottingham for funding of this research. MJC acknowledges the support of the School of Chemistry, University of Nottingham for the award of a Hobday Fellowship. We gratefully acknowledge Dr. Flavia Pop for providing some starting materials.

References

[1] G. Zhang, H. Li, S. Bi, L. Song, Y. Lu, L. Zhang, J. Yu, L. Wang, Analyst, 2013, 138, 6163-6170.

[2] L. Wang, J. Du, D. Cao, Sensors and Actuators B, 2014, 198, 455–461.

[3] M. Kaur, D.H. Choi, Chem. Soc. Rev., 2015, 44, 58-77.

[4] W. Li, L. Wang, H. Tang, D. Cao, Dyes and Pigments, 2019, 162, 934-950.

[5] S. Qua, H. Tian, Chem. Commun., 2012, 48, 3039-3051

[6] Y. Li, P. Sonar, L. Murphy, W. Hong, Energy Environ. Sci., 2013, 6, 1684-1710.

[7] H. Choi, S. J. Ko, T. Kim, P. O Morin, B. Walker, B. H.Lee, M. Leclerc, J. Y. Kim, A. J. Heeger, Adv. Mater., 2015, 21, 3318-3324.

[8] A. Tang, C. Zhan, J. Yao, E. Zhou, Adv. Mater. 2017, 29, 1600013.

[9] Ch Zhao, Y. Guo, Y. Zhang, N. Yan, S. You, W. Li, J. Mater. Chem. A, 2019, 7, 10174-10199.

[10] X. He, L. Yin, Y. Li, J. Mater. Chem. C, 2019, 7, 2487-2521.

[11] E. Ripaud, D. Demeter, T. Rousseau, E. Boucard-Cétol, M. Allain, Ri. Po, P. Leriche, J. Roncali, Dyes and Pigments, 2012, 95, 126-133.

[12] A. Iqbal, M. Jost, R. Kirchmayr, J. Pfenninger, A. Rochat, O. Wallquist, Bull. Soc. Chim. Belg., 1988, 97, 615-643.

[13] M. Grzybowski, D.T. Gryko, Adv. Optical Mater., 2015, 3, 280-320.

[14] J. Calvo-Castro, S. Maczka, C. Thomson, G. Morris, A. R. Kennedy, C. J. McHugh, CrystEngComm, 2016, 18, 9382–9390.

[15] P. Josse, C. Dalinot, Y. Jiang, S. Dabos-Seignon, J. Roncali, P. Blanchard, C. Cabanetos, J. Mater. Chem. A, 2016, 4, 250-256.

[16] J. Huang, X. Liu, D. Gao, C. Wei, W. Zhang, G. Yu, RSC Adv., 2016, 6, 83448-83455.

[17] M. Grzybowski, E. Glodkowska-Mrowka, T. Stoklosa, D.T. Gryko, Org. Lett., 2012, 14, 2670-2673.

[18] G. Colonna, T. Pilati, F. Rusconi, G. Zecchi, Dyes Pigm.,, 2007, 75, 125-129.

[19] A.R. Rabindranath, Y. Zhu, I. Heim, B. Tieke, Macromolecules, 2006, 39, 8250–8256.

[20] S.H. Choi, O.T. Kwon, N. R. Kim, C. Yoon, J.P. Kim, J.H. Choi, Bull. Korean Chem. Soc., 2010, 31, 1073-1076.

[21] V.S. Gevaerts, E.M. Herzig, M. Kirkus, K.H. Hendriks, M.M. Wienk, J. Perlich, P. Müller-Buschbaum, R.A.J. Janssen, Chem. Mater., 2014, 26, 916−926.

[22] K. Nie, S. Xu, X. Duan, H. Shi, B. Dong, M. Long, H. Xu, X. F. Jiang, Z. Liu, Sensors and Actuators B, 2018, 265, 1–9.

[23] S. Luňák Jr., M. Vala, Jan Vyňuchal, I. Ouzzane, P. Horáková, P. Možíšková, Z. Eliáš, M. Weiter, Dyes and Pigments, 2011, 91, 269-278.

[24] Z, Liu, G. Zhang, D. Zhang, Acc. Chem. Res., 2018, 51, 1422-1432.

[25] J. Dhar, N. Venkatramaiah, Anitha A, S. Patil, J. Mater. Chem. C, 2014, 2, 3457-3466.

[26] P. M. Beaujuge, C. M. Amb, J. R. Reynolds, Acc. Chem. Res., 2010, 43, 1396–1407.

[27] K. Chung, A. McAllister, D. Bilby, B.-G. Kim, M. S. Kwon, E. Kioupakis, J. Kim, Chem. Sci., 2015, 6, 6980-6985.

[28] H. Bürckstümmer, A. Weissenstein, D. Bialas, F. Würthner, J. Org. Chem., 2011, 76, 2426-2432.

[29] G. Colonna, T. Pilati, F. Rusconi, G. Zecchi, Dyes Pigm., 2007, 75, 125–129.

[30] G. Zhang, L. Song, S. Bi, Y. Wu, J. Yu, L. Wang, Dyes Pigm., 2014, 102, 100–106.

[31] E. Heyer, P. Lory, J. Leprince, M. Moreau, A. Romieu. M. Guardigli, A. Roda, R. Ziessel, Angew. Chem. Int. Ed., 2015, 54, 2995-2999.

[32] D. Hablot P. Retailleau, R. Ziessel, Chem. Eur. J., 2010, 16, 13346-13351

[33] F. Pop, W. Lewis, D. B. Amabilino, Cryst Eng Comm, 2016, 18, 8933–8943.

[34] I. Ohnishi, K. Hashimoto, K. Tajima, R. Soc. Open Sci. 2018, 5, 172025.

[35] S. Stas, J. Y. Balandier, V. Lemaur, O. Fenwick, Y. H. Geerts., Dyes Pigm., 2013, 97, 198-208.

[36] A. Shaabani, M. Dabiri, A. Bazgir, K. Gharanjig, Dyes and Pigments, 2006, 71, 68- 72.

[37] P. Sonar, G. M. Ng, T. T Lin, A. Dodabalapura, Z. K. Chen., J. Mater. Chem., 2010, 20, 3626–3636.

[38] F. Pop, J. Humphreys, J. Schwarz, L. Brown, A. van den Berg, D.B. Amabilino, New J. Chem., 2019, 43, 5783-5790.

[39] A.B. Tamayo, M. Tantiwiwat, B. Walker, T.-Q. Nguyen, J. Phys. Chem. C, 2008, 112, 15543–15552.

[40] S. Luňák Jr., Z. Eliáš, T. Mikyseka, J. Vyňuchal, J. Ludvík, Electrochim. Acta, 2013, 106, 351-359.

[41] P. Data, A. Kurowska, S. Pluczyk, P. Zassowski, P. Pander, R. Jedrysiak, M. Czwartosz, L. Otulakowski, J. Suwinski, M. Lapkowski, A.P. Monkman, J. Phys. Chem. C, 2016, 120, 2070-2078.

[42] J. Mizuguchi, Ber. Bunsenges. Phys. Chem., 1993, 97, 693-701.

[43] A. D. Becke, Phys. Rev. A, 1988, 38, 3098-3100.

[44] C. Lee, W. Yang, R. G. Parr, Phys. Rev.B, 1988, 37, 785-789.

[45] A. D. Becke, J. Chem. Phys., 1993, 98, 5648-5652.

[46] Gaussian 09, Revision D.01, M. J. Frisch, G. W. Trucks, H. B. Schlegel, G. E. Scuseria, M. A. Robb, J. R. Cheeseman, G. Scalmani, V. Barone, B. Mennucci, G. A. Petersson, H. Nakatsuji, M. Caricato, X. Li, H. P. Hratchian, A. F. Izmaylov, J. Bloino, G. Zheng, J. L. Sonnenberg, M. Hada, M. Ehara, K. Toyota, R. Fukuda, J. Hasegawa, M. Ishida, T. Nakajima, Y. Honda, O. Kitao, H. Nakai, T. Vreven, J. A. Montgomery, Jr., J. E. Peralta, F. Ogliaro, M. Bearpark, J. J. Heyd, E. Brothers, K. N. Kudin, V. N. Staroverov, T. Keith, R. Kobayashi, J. Normand, K. Raghavachari, A. Rendell, J. C. Burant, S. S. Iyengar, J. Tomasi, M. Cossi, N. Rega, J. M. Millam, M. Klene, J. E. Knox, J. B. Cross, V. Bakken, C. Adamo, J. Jaramillo, R. Gomperts, R. E. Stratmann, O. Yazyev, A. J. Austin, R. Cammi, C. Pomelli, J. W. Ochterski, R. L. Martin, K. Morokuma, V. G. Zakrzewski, G. A. Voth, P. Salvador, J. J. Dannenberg, S. Dapprich, A. D. Daniels, O. Farkas, J. B. Foresman, J. V. Ortiz, J. Cioslowski, and D. J. Fox, Gaussian, Inc., Wallingford CT, 2013.

[47] B. Walker, J. Liu, C. Kim, G. C. Welch, J. K. Park, J. Lin, P. Zalar, C. M. Proctor, J. H. Seo, G. C. Bazana, T. Q. Nguyen., Energy Environ. Sci., 2013, 6, 952–962.

[48] A. D. Hendsbee, J. P. Sun, L. R. Rutledge, I. G. Hill, G. C. Welch., J. Mater. Chem. A, 2014, 2, 4198–4207.

[49] J. Mizuguchi, A.C. Rochat, Ber. Bunsenges. Phys. Chem., 1992, 96, 708-711.

[50] M. Gora, S. Pluczyk, P. Zassowski, W. Krzywiec, M. Zagorska, J. Mieczkowski, M. Lapkowski, A. Pron, Synthetic Metals, 2016, 216, 75–82.

[51] M. Vala, M.Weiter, J. Vynuchal, P. Toman, S. Lunák, J Fluoresc, 2008, 18, 1181–1186.

[52] T. Potrawa, H. Langhals, Chem. Ber., 1987, 120, 1075-1078.

[53] N. L. C. Leung, N. Xie. W. Yuan, Y. Liu, Q. Wu, Q. Peng, Q. Miao, J.W. Y. Lam, B. Z Tang, Chem. Eur. J., 2014, 20, 15349–15353.

[54] S. Dong, Z. Li, J. Qin, J. Phys. Chem. B, 2009, 113, 434–441.

[55] Y. Jin, Y. Xu, Y. Liu, L. Wang, H. Jiang, X. Li, D. Cao, Dyes and Pigments, 2011, 90, 311- 318.

[56] K. Gutkowski, C. Azarias, M. Banasiewicz, B. Kozankiewicz, D. Jacquemin, D.T. Gryko, Eur. J. Org. Chem. 2018, 6643–6648.

[57] O. Vakuliuk, A. Purc, G. Clermont, M. Blanchard-Desce, D.T. Gryko, ChemPhotoChem, 2017, 1, 243-252.

[58] J. Kuwabara, T. Yamagata, T. Kanbara, Tetrahedron, 2010, 66, 3736-3741.

[59] H. Langhals, T. Potrawa, H. Nöth, G. Linti, Angew. Chem. Int. Ed., 1989, 28, 478-480.

[60] J. Calvo-Castro, C. J. McHugh, J. Mater. Chem. C, 2017, 5, 3993-3998.

[61] M. A. Naik, N. Vnekatramaiah, C. Kanimozhi, S. Patil, J. Phys. Chem. C, 2012, 116, 26128-26137.

[62] R. Wawrzinek, X. Zhou, M. Ullah, E. Namdas, S.C. Lo, Dyes and Pigments, 2017, 136, 678-685.

[63] B.R. Gautam, R. Younts, J. Carpenter, H. Ade, K. Gundogdu, J. Phys. Chem. A, 2018, 122, 3764-3771.

[64] M. Montoya, R. Janssen, Adv. Funct. Mater., 2017, 27, 1605779.

Supporting information for:

Ground and excited states of bis-4-methoxybenzyl diketopyrrolopyrroles

Alanna S. Murphy,[a,b] Catherine E. Killalea,[a,b] Joshua Humphreys,[a,b] Paul A. Hume, [a,b]§ Matthew J. Cliffe,[b] E. Stephen Davies,[b] William Lewis[b]¶ and David B. Amabilino*[a,b]

a GSK Carbon Neutral Laboratories for Sustainable Chemistry, The University of Nottingham, Triumph Road, Nottingham, NG7 2TU, UK.

b School of Chemistry, The University of Nottingham, NG7 2RD Nottingham, UK

§ Present address MacDiarmid Institute for Advanced Materials and Nanotechnology and School of Chemical and Physical Sciences, Victoria University of Wellington, Wellington 6010, New Zealand

¶Present address Chemistry Building, The University of Sydney, Eastern Avenue NSW 2006, Australia

Contents

1. Synthetic methods

General techniques and characterization: Column chromatography purifications were carried out using silica gel (Sigma Aldrich, 60 Å pore size and 40- 63 μm particle size. All synthetic procedures were carried out under an inert atmosphere (unless stated otherwise, see supporting information for details). NMR spectra were acquired on a Bruker 400 or 500 MHz and recorded at room temperature. ^{1}H and ^{13}C were referenced to the solvent residual peak. The abbreviations used for peak multiplicities are as follows: s, singlet; d, doublet; t, triplet; dd, doublet of doublets; m, multiplet and br, broad. MALDI- ToF MS was carried out using Bruker UltraFlex (III) with *trans*-2-[3-(4-*tert*-butylphenyl)-2-methyl-2-propenylidene] malononitrile (DCTB) as matrix. Elemental analysis (CHN) was performed by the University of Nottingham, School of Chemistry Microanalytical Service using an Exeter Analytical CE-440 instrument. Infrared spectroscopy was carried out on a Bruker ATR-IR.

1.1 4MB ThDPP: The parent ThDPP (1.5 g, 5 mmol) was dissolved in dimethylformamide (anhydrous, 20 ml) and potassium carbonate (1.38g, 10 mmol) was added and the reaction was stirred at 80 ^{o}C for 30 mins. 4- methoxybenzyl chloride

(1.45 ml, 10 mmol) was added in 1 portion and the reaction was stirred at reflux for 24 hours. The reaction was cooled to room temperature and deionised water was added causing precipitation. The suspension was filtered and washed with water and methanol. The solid was washed with dichloromethane and the filtrate was dried in vacuo. The crude product was purified by column chromatography on silica gel using dichloromethane: hexane (10%) to give the final product as a purple powder. (55%). ^{1}H NMR ($CDCl_3$, 400 MHz); δH 3.79 (6H, s), 5.33 (4H, d), 6.87 (4H, dd), 7.20 (4H, dd), 7.22 (2H, t), 7.59 (2H, d), 8.74 (2H, d) ppm; ^{13}C NMR ($CDCl_3$, 100 MHz); δ 161.16, 158.86, 140.45, 135.02, 131.33, 129.56, 128.84, 128.47, 127.62, 114.17, 107.71, 55.26, 44.87 ppm, elemental analysis calcd for $C_{30}H_{24}N_2O_4S_2$: C, 66.65; H, 4.47; N, 5.18%; found: C, 66.33; H, 4.26; N, 5.02%, mass calcd. 540.12, found (MALDI ToF) m/z = 539.71 (100%),

NMR Spectra for **4MB ThDPP**

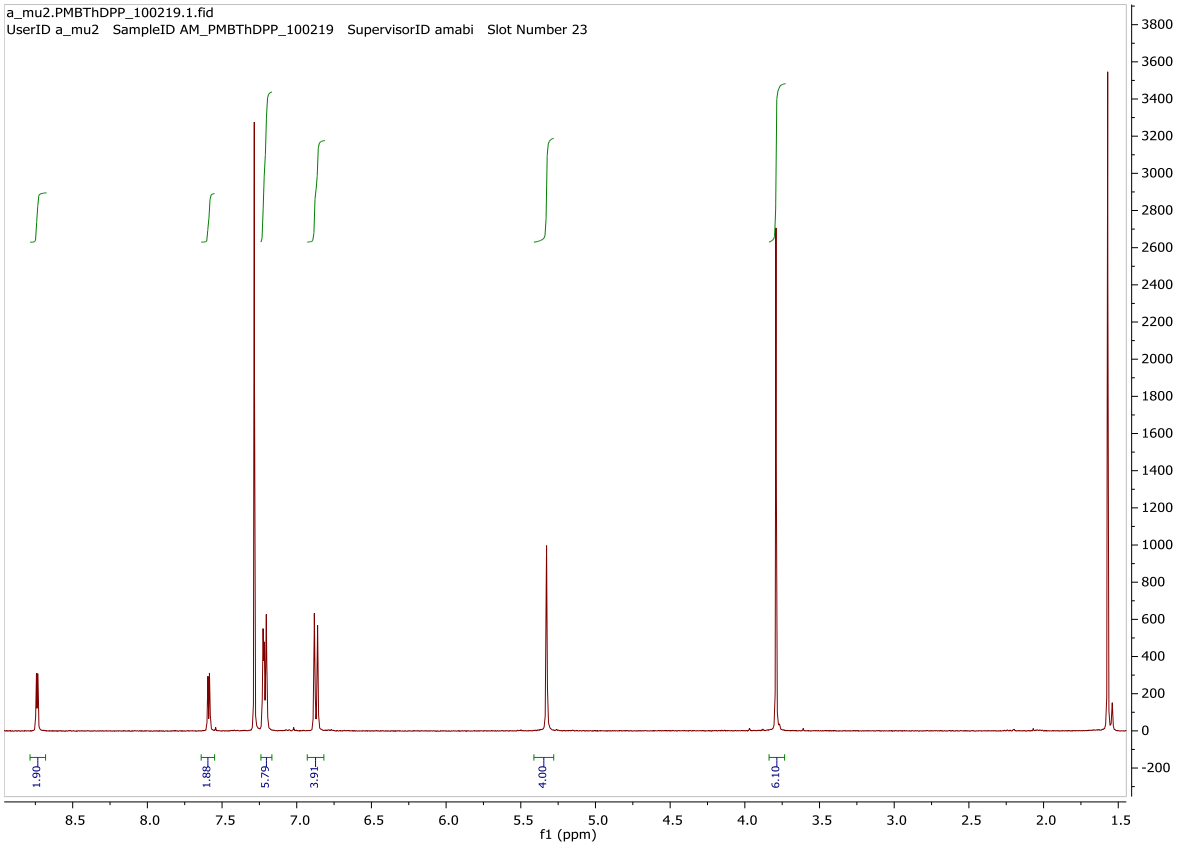

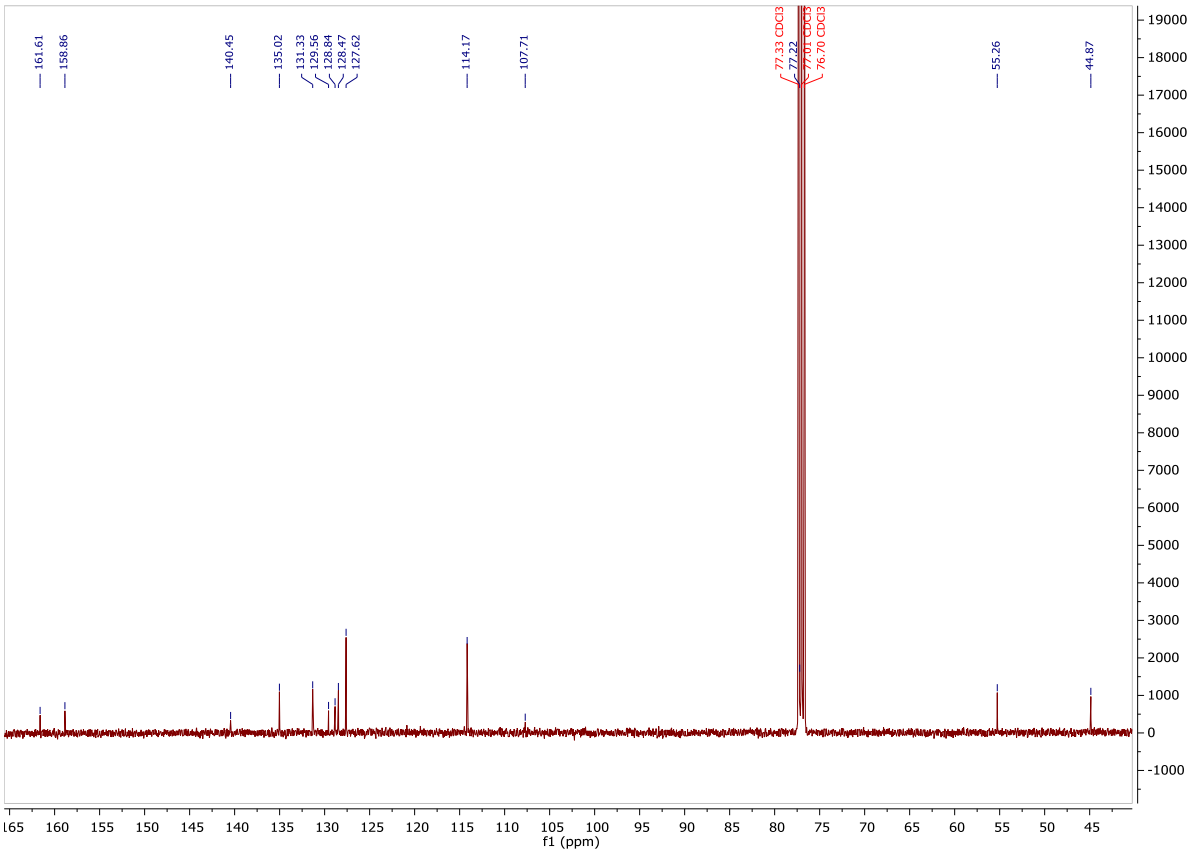

1.2 4MB OMePhDPP: The parent OMePhDPP (650 mg, 1.87 mmol) was dissolved in acetonitrile (anhydrous, 60ml) and caesium carbonate (1.22 g, 3.75 mmol) was added.

The mixture was stirred and heated to reflux for 2 hours. 4- methoxybenzyl chloride (586 mg, 3.75 mmol) was added in 1 portion and the mixture was stirred at reflux for 12 hours. The reaction mixture was cooled and the solvent removes in vacuo. The crude solid material was sonicated in deionised water and methanol (1:1) and filtered by suction. The solid was washed successively with cold acetonitrile, water and methanol. The solid was washed and dissolved with dichloromethane and the filtrate was collected, the solvent was removed in vacuo yielding the final product as a bright orange powder. (57%). ^{1}H NMR ($CDCl_3$, 400 MHz); δH 3.80 (6H, s br), 3.87 (6H, s br), 4.96 (2H, s br), 6.85 (4H, d), 6.79 (4H, d), 7.16 (4H, d), 7.80 (4H, d) ppm; ^{13}C NMR ($CDCl_3$, 100 MHz); δ 163.06, 161.93, 158.79, 131.06, 129.84, 127.99, 120.56, 114.30, 114.15, 55.45, 55.27, 45.14 ppm, elemental analysis calcd for $C_{36}H_{32}N_2O_6$: C, 73.45; H, 5.48; N, 4.76%; found: C, 72.38; H, 5.36; N, 4.26%, mass calcd. 588.23, found (MALDI ToF) m/z = 587.87 (100%),

NMR Spectra for **4MB OMePhDPP**

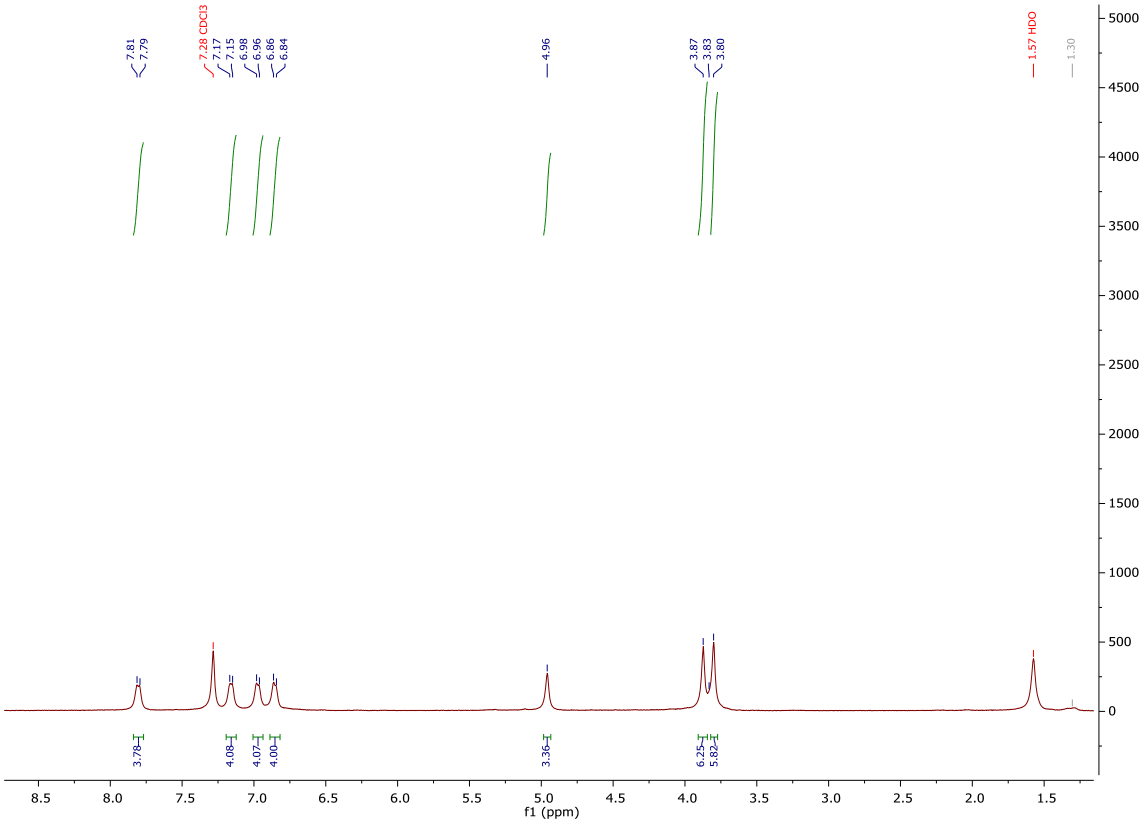

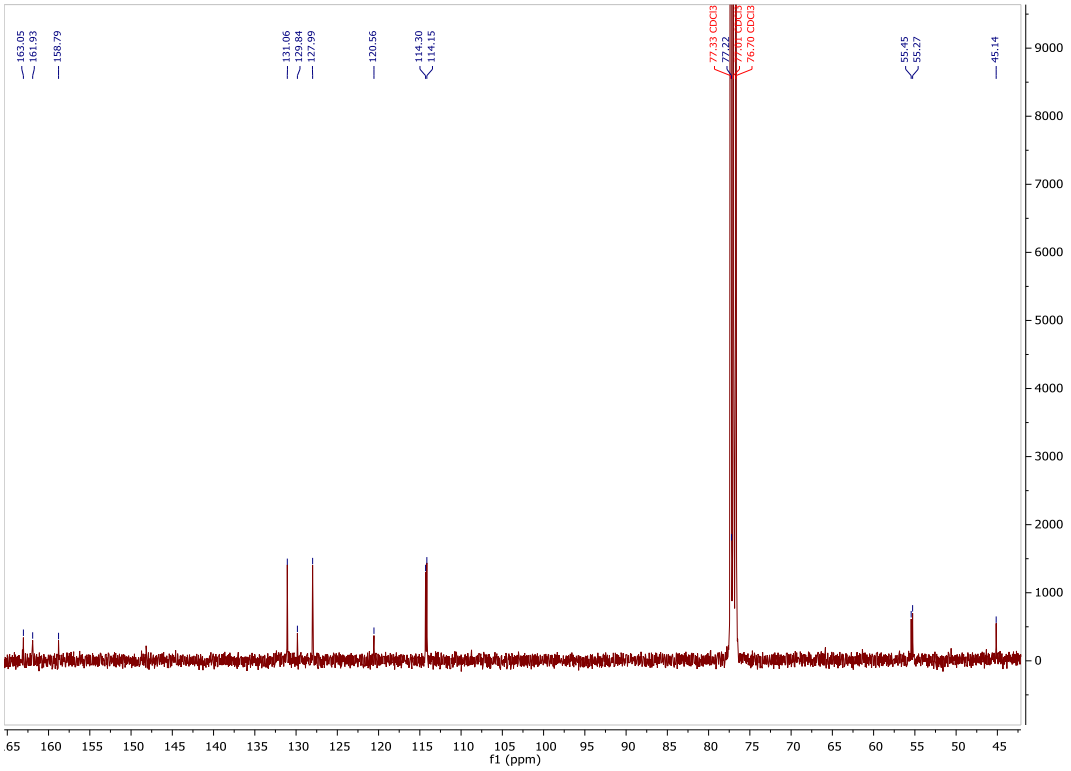

1.3 4MB ThPhDPP: The parent ThPh-PyDPP (with pyran protecting group on phenol) (1.01 mmol) and caesium carbonate (4.05 mmol) were stirred at 90 °C in acetonitrile (40 mL) for 15 min. 4- methoxybenzyl chloride (634 mg, 4.05 mmol) was then added to the reaction mixture, which was stirred at 90 °C for 24 h. The reaction mixture was cooled to room temperature, water was added (40 mL). The product was extracted with dichloromethane (3 x 15 mL) and washed with water (3 x 15 ml), dried over $MgSO_4$, filtered and the solvent was removed under reduced pressure. The crude protected product was purified by column chromatography on silica gel using dichloromethane: ethyl acetate (2%). The protected pure product was dissolved in dichloromethane and then stirred in 6 M HCl until precipitation occurred. The solid was filtered and washed with water, methanol and diethyl ether to give the product as a bright red solid. (40%), ^{1}H NMR (DMSO-d^6, 400 MHz,) δ 3.71 (d, J = 3.3 Hz, 6H), 5.00 (s, 2H), 5.18 (s, 2H), 6.94 – 6.81 (m, 7H), 7.18 – 7.01 (m, 4H), 7.31 (dd, J = 5.0, 3.9 Hz, 1H), 7.84 – 7.67 (m, 2H), 7.99 (dd, J = 5.0, 1.2 Hz, 1H), 8.61 (dd, J = 3.9, 1.2 Hz, 1H), (solubility is too poor to allow ^{13}C NMR with sufficient signal to noise near room temperature). elemental analysis calcd for $C_{32}H_{26}N_2O_5S$: C, 69.80; H, 4.76; N, 5.09%; found: C, 68.65; H, 4.52; N, 4.91%, mass calcd. 550.16, found (MALDI ToF) m/z = 550.80 (100%),

^{1}H NMR Spectrum for **4MB ThPhDPP**

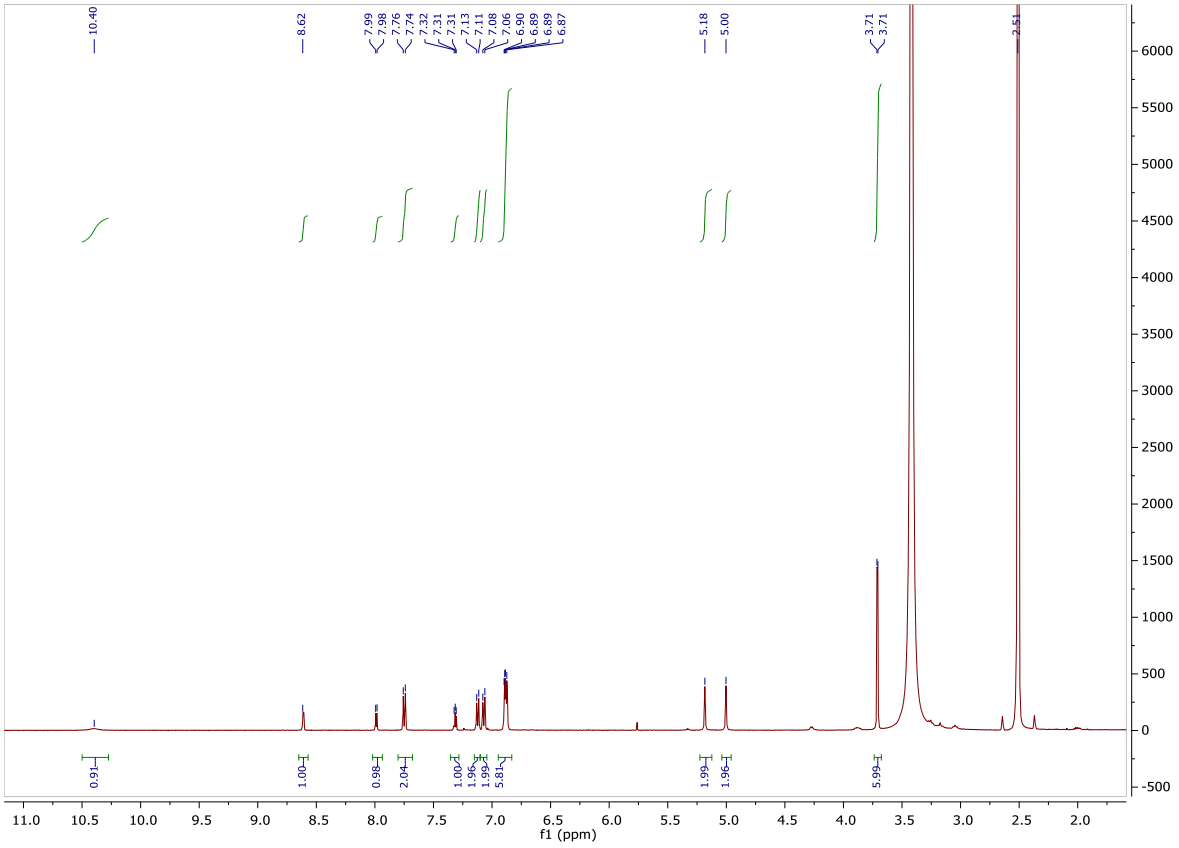

2. Electrochemical data

Scan rate dependence for 4MB ThDPP

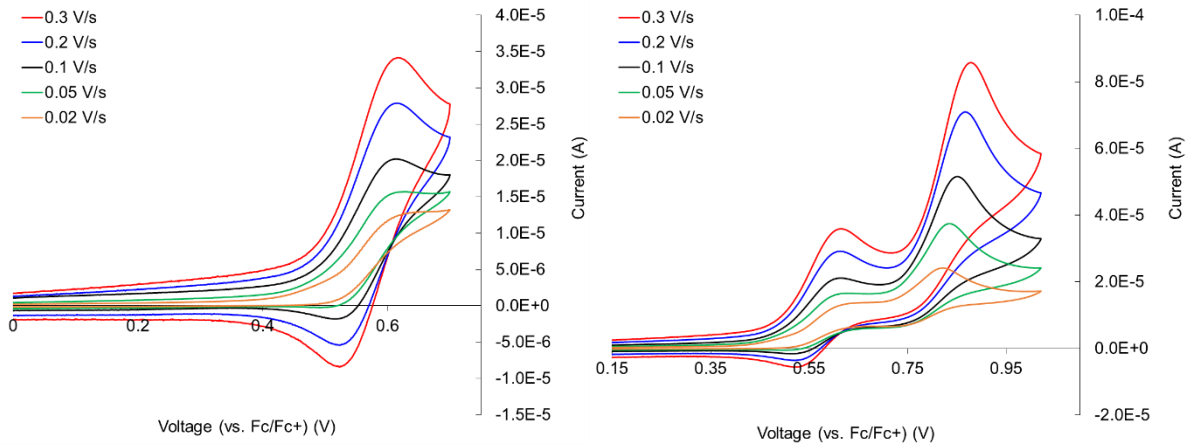

Figure SI1. Cyclic Voltammetry of 4MB ThDPP showing the effect of scan rate on the first (left) and second (right) oxidation processes. In CH_2Cl_2 containing $[nBu_4N][PF_6]$ (0.2 M) as supporting electrolyte, at ambient temperature. Potentials are plotted against $E_{1/2}$ Fc^+/Fc used as the internal standard.

Table SI1. The effect of scan rate on anodic and cathodic peak potentials for the first and second oxidation processes of 4MB ThDPP. In CH_2Cl_2 containing [n-Bu_4N][PF_6] (0.2 M) as supporting electrolyte, at ambient temperature. Potentials are quoted against $E_{1/2}$ Fc^+/Fc used as the internal standard.

Scan Rate / Vs^{-1}	**E_{pa} (1^{st} ox) / V**	**E_{pc} (1^{st} ox) / V**	**E_{pa-pc} (1^{st} ox) / V**	**$E_{1/2}$ (1^{st} ox) / V**	**E_{pa} (2^{nd} ox) / V**	**E_{pc} (2^{nd} ox) / V**	**E_{pa-pc} (2^{nd} ox) / V**	**$E_{1/2}$ (2^{nd} ox) / V**	**E_{pa-pc} Fc^+/Fc / V**
0.30	0.62	0.53	0.09	0.58	0.88	n/a	n/a	n/a	0.08
0.20	0.62	0.53	0.09	0.58	0.87	n/a	n/a	n/a	0.08
0.10	0.62	0.53	0.09	0.58	0.85	n/a	n/a	n/a	0.08
0.05	0.63	n/a	n/a	n/a	0.84	n/a	n/a	n/a	0.07
0.02	n/a	n/a	n/a	n/a	0.82	n/a	n/a	n/a	0.07

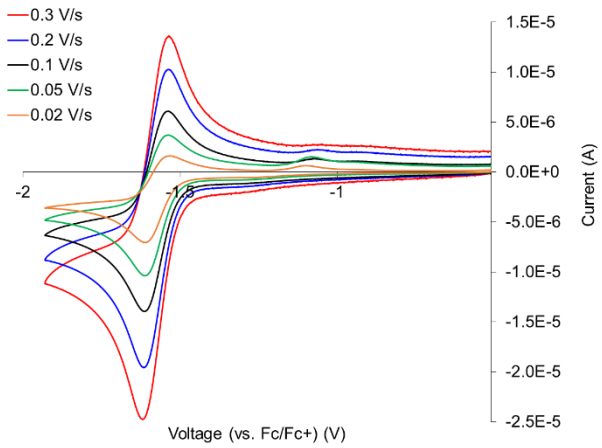

Figure SI2. Cyclic Voltammetry of 4MB ThDPP showing the effect of scan rate on the reduction process. In CH_2Cl_2 containing [n-Bu_4N][PF_6] (0.2 M) as supporting electrolyte, at ambient temperature. Potentials are plotted against $E_{1/2}$ Fc^+/Fc used as the internal standard.

Table SI2. The effect of scan rate on anodic and cathodic peak potentials for the first reduction process of 4MB ThDPP. In CH_2Cl_2 containing [n-Bu_4N][PF_6] (0.2 M) as supporting electrolyte, at ambient temperature. Potentials are quoted against $E_{1/2}$ Fc^+/Fc used as the internal standard.

Scan Rate /Vs^{-1}	**E_{pa} (1st red) / V**	**E_{pc} (1st red) / V**	**E_{pa-pc} (1st red) / V**	**$E_{1/2}$ (1st red) / V**	**E_{pa-pc} Fc^+/Fc /V**
0.30	-1.62	-1.53	0.09	-1.58	0.08
0.20	-1.61	-1.54	0.07	-1.58	0.08
0.10	-1.61	-1.54	0.07	-1.58	0.08
0.05	-1.61	-1.54	0.07	-1.58	0.07
0.02	-1.61	-1.53	0.08	-1.57	0.07

Scan rate dependence for 4MB OMePhDPP

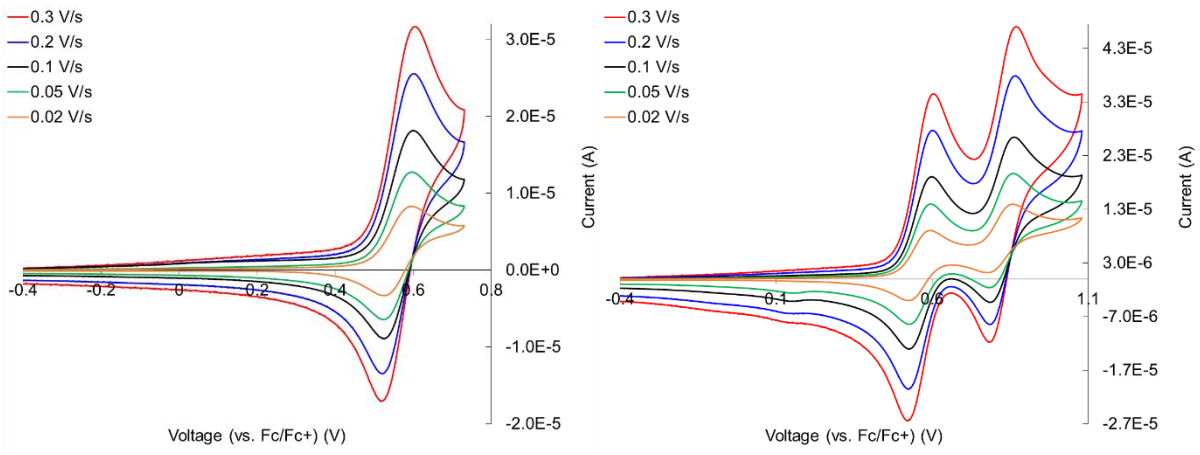

Figure SI3. Cyclic Voltammetry of 4MB OMePhDPP showing the effect of scan rate on the first (left) and second (right) oxidation processes. In CH_2Cl_2 containing [n-Bu_4N][PF_6] (0.2 M) as supporting electrolyte, at ambient temperature. Potentials plotted against $E_{1/2}$ Fc^+/Fc used as the internal standard.

Table SI3. The effect of scan rate on anodic and cathodic peak potentials for the first and second oxidation processes of 4MB OMePhDPP. In CH_2Cl_2 containing [n-Bu_4N][PF_6] (0.2 M) as supporting electrolyte, at ambient temperature. Potentials are quoted against $E_{1/2}$ Fc^+/Fc used as the internal standard.

Scan Rate / Vs^{-1}	**E_{pa} (1^{st} ox) / V**	**E_{pc} (1^{st} ox) / V**	**E_{pa-pc} (1^{st} ox) / V**	**$E_{1/2}$ (1^{st} ox) / V**	**E_{pa} (2^{nd} ox) / V**	**E_{pc} (2^{nd} ox) / V**	**E_{pa-pc} (2^{nd} ox) / V**	**$E_{1/2}$ (2^{nd} ox) / V**	**E_{pa-pc} Fc^+/Fc /V**
0.30	0.62	0.53	0.09	0.58	0.88	0.80	0.08	0.84	0.07
0.20	0.61	0.53	0.08	0.57	0.88	0.80	0.08	0.84	0.07
0.10	0.61	0.54	0.07	0.58	0.88	0.80	0.08	0.84	0.07
0.05	0.61	0.54	0.07	0.58	0.87	0.80	0.07	0.84	0.07
0.02	0.61	0.54	0.07	0.58	0.87	0.79	0.08	0.83	0.07

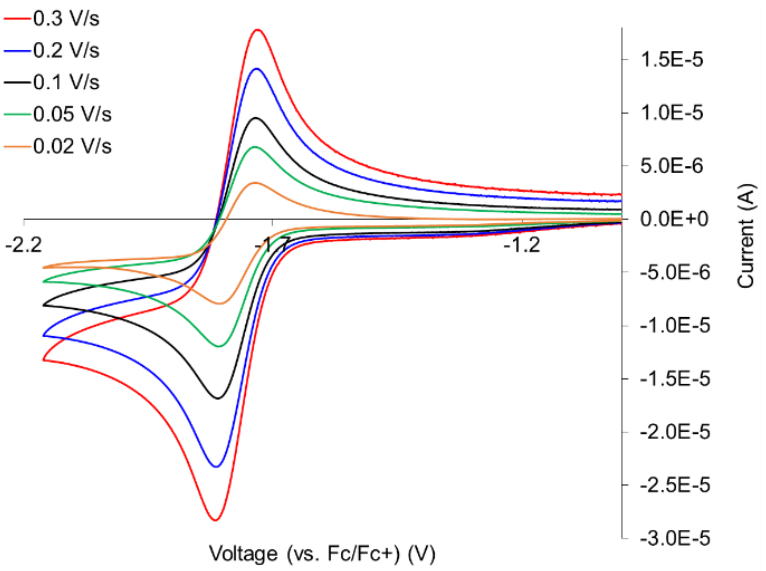

Figure SI4. Cyclic Voltammetry of 4MB OMePhDPP showing the effect of scan rate on the reduction process. In CH_2Cl_2 containing [n-Bu_4N][PF_6] (0.2 M) as supporting electrolyte, at ambient temperature. Potentials are plotted against $E_{1/2}$ Fc^+/Fc used as the internal standard.

Table SI4. The effect of scan rate on anodic and cathodic peak potentials for 4MB OMePhDPP. In CH_2Cl_2 containing [n-Bu_4N][PF_6] (0.2 M) as supporting electrolyte, at ambient temperature. Potentials are quoted against $E_{1/2}$ Fc^+/Fc used as the internal standard.

Scan Rate /Vs^{-1}	**E_{pa} (1^{st} red) / V**	**E_{pc} (1^{st} red) / V**	**E_{pa-pc} (1^{st} red) / V**	**$E_{1/2}$ (1^{st} red) / V**	**E_{pa-pc} Fc^+/Fc /V**
0.30	-1.80	-1.72	0.08	-1.76	0.07
0.20	-1.80	-1.72	0.08	-1.76	0.07
0.10	-1.80	-1.72	0.08	-1.76	0.07
0.05	-1.80	-1.72	0.08	-1.76	0.07
0.02	-1.80	-1.72	0.08	-1.76	0.07

Scan rate dependence for 4MB ThPhDPP

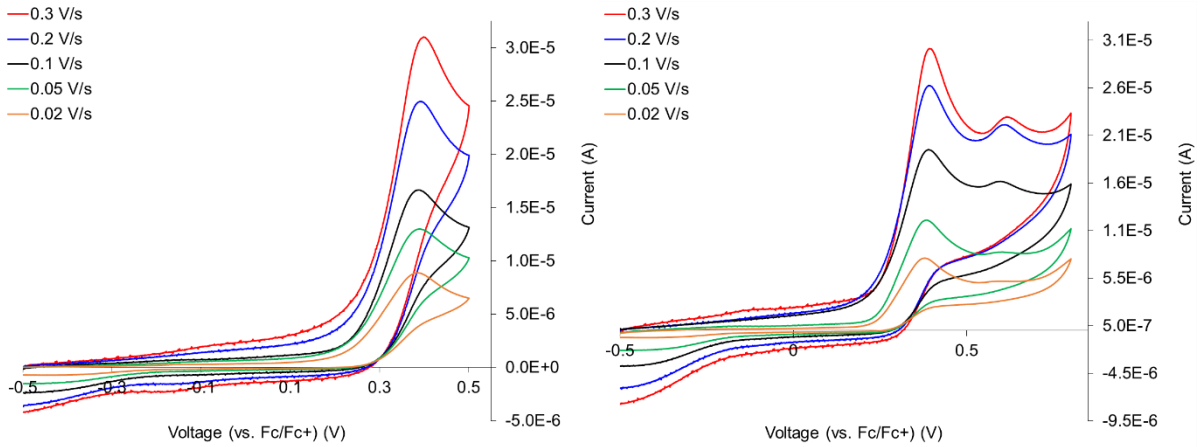

Figure SI5. Cyclic Voltammetry of 4MB ThPhDPP showing the effect of scan rate on the first (left) and second (right) oxidation processes. In DMF containing [n-Bu$_4$N][PF$_6$](0.1 M) as supporting electrolyte, at ambient temperature. Potentials plotted against $E_{1/2}$ Fc^+/Fc used as the internal standard.

Table SI5. The effect of scan rate on anodic peak potentials for 4MB ThPhDPP. In DMF containing [n-Bu$_4$N][PF$_6$] (0.1 M) as supporting electrolyte, at ambient temperature. Potentials quoted against $E_{1/2}$ Fc^+/Fc used as the internal standard.

Scan Rate / Vs^{-1}	**E_{pa} (1^{st} ox) / V**	**E_{pc} (1^{st} ox) / V**	**E_{pc} (2^{nd} ox) / V**	**E_{pa} (2^{nd} ox) / V**
0.30	0.41	n/a	0.63	n/a
0.20	0.40	n/a	0.62	n/a
0.10	0.39	n/a	0.61	n/a
0.05	0.40	n/a	0.61	n/a
0.02	0.39	n/a	0.60	n/a

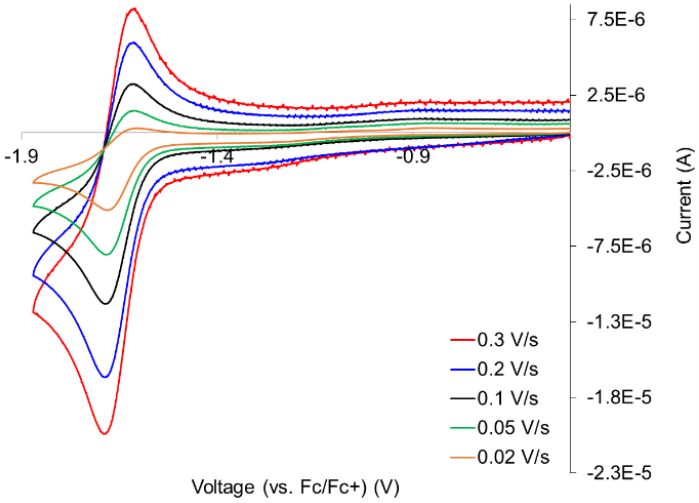

Figure SI6. Cyclic Voltammetry of 4MB ThPhDPP showing the effect of scan rate on the reduction process. In DMF containing [n-Bu$_4$N][PF$_6$] (0.1 M) as supporting electrolyte, at ambient temperature. Potentials plotted against $E_{1/2}$ Fc$^+$/Fc used as the internal standard.

Table 6. The effect of scan rate on anodic and cathodic peak potentials for 4MB ThPhDPP. In DMF containing [n-Bu$_4$N][PF$_6$] (0.1 M) as supporting electrolyte, at ambient temperature. Potentials quoted against $E_{1/2}$ Fc$^+$/Fc used as the internal standard.

Scan Rate / Vs^{-1}	**E_{pa} (1st red) / V**	**E_{pc} (1st red) / V**	**E_{pa-pc} (1st red) / V**	**$E_{1/2}$ (1st red) / V**	**E_{pa-pc} Fc$^+$/Fc /V**
0.30	-1.68	-1.61	0.07	-1.64	0.08
0.20	-1.68	-1.61	0.07	-1.64	0.07
0.10	-1.68	-1.61	0.07	-1.64	0.07
0.05	-1.68	-1.61	0.07	-1.64	0.07
0.02	-1.67	-1.60	0.07	-1.64	0.07

Full cyclic voltammogram for Hex OMePhDPP

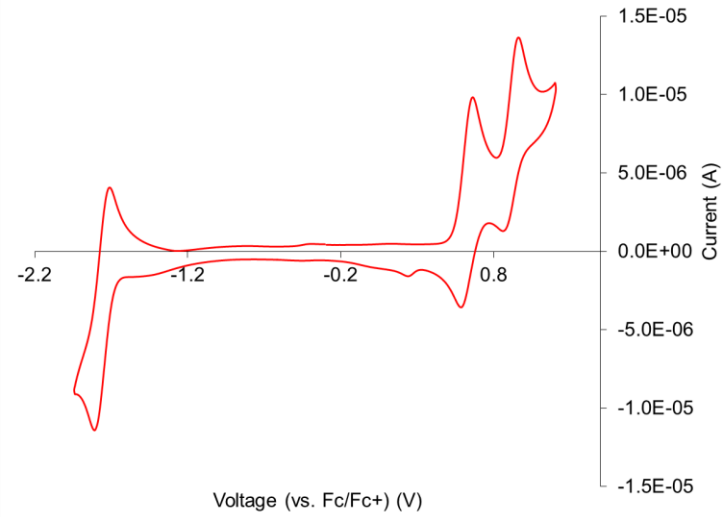

Figure SI7. Full CV of Hex OMePhDPP, referenced against the potential of Fc/Fc+.

Full cyclic voltammogram for Hex ThPhDPP

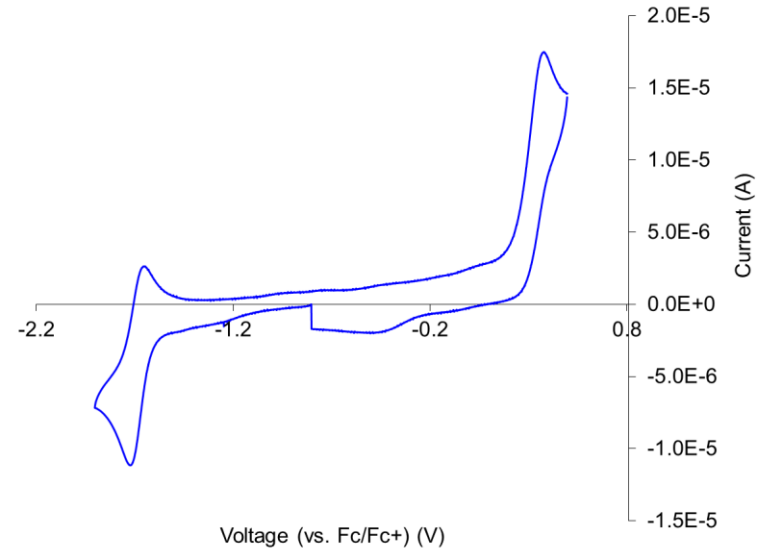

Figure SI8. Full CV of Hex ThPhDPP, referenced against the potential of Fc/Fc+.

3. Spectroelectrochemical data

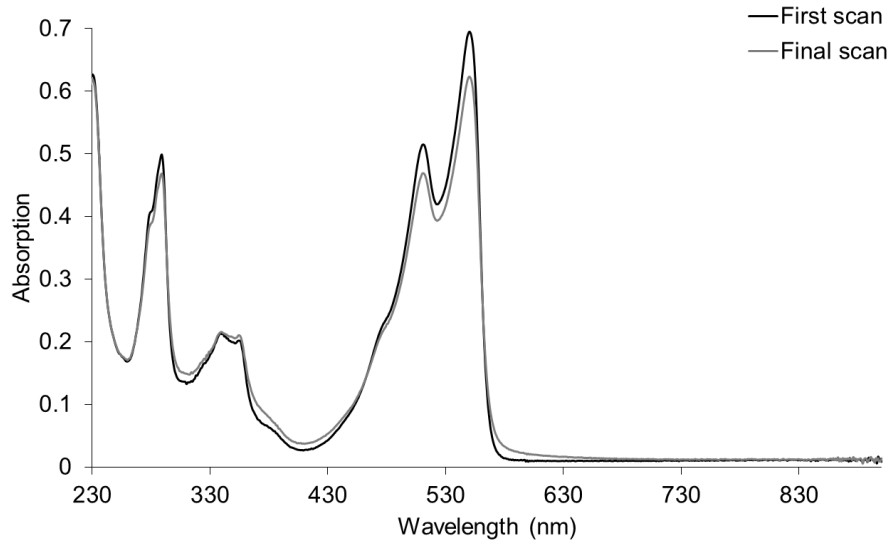

Figure SI9. UV-visible absorption spectra of PMB ThDPP (first scan) and after the oxidation cycle (final scan). Spectra were recorded in CH_2Cl_2 containing [n-Bu_4N][PF_6] (0.2 M) as the supporting electrolyte at 273 K.

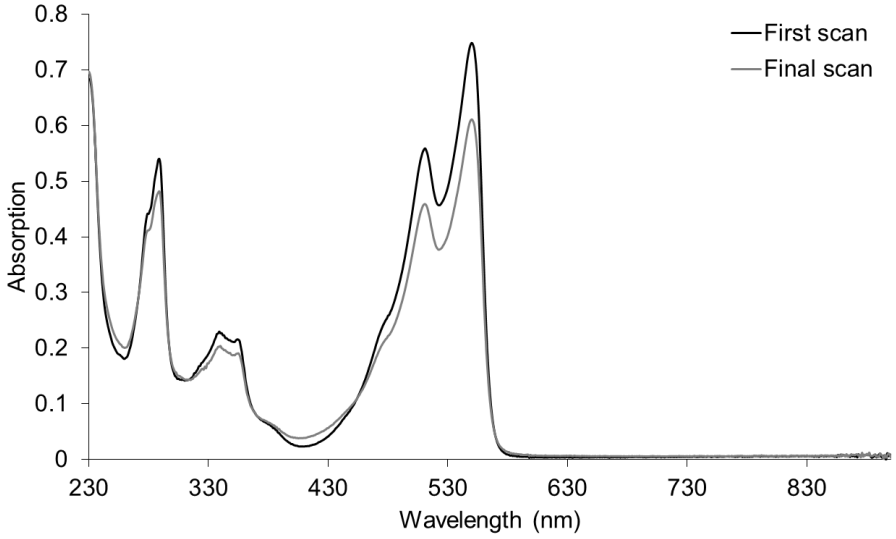

Figure SI10. UV-visible absorption spectra of PMB ThDPP (first scan) and after the reduction cycle (final scan). Spectra were recorded in CH_2Cl_2 containing [n-Bu_4N][PF_6] (0.2 M) as the supporting electrolyte at 273 K.

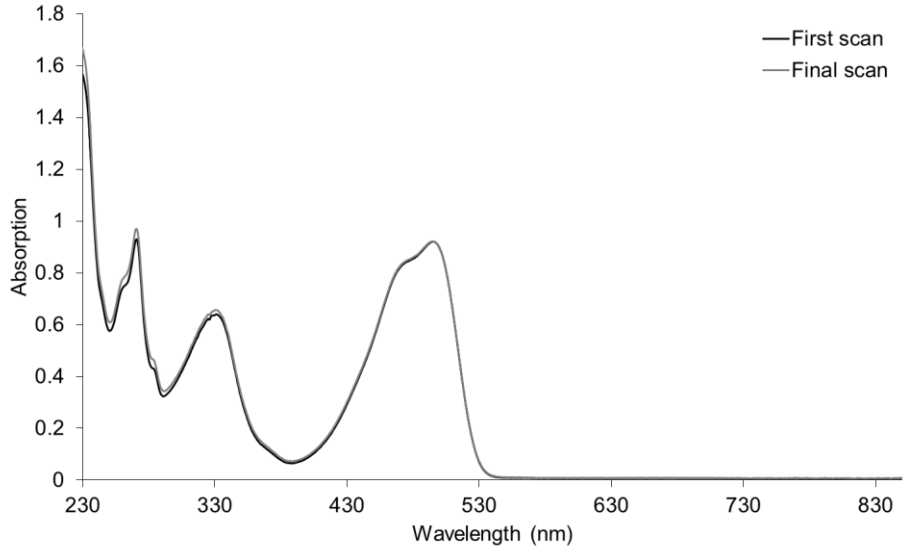

Figure SI11. UV-visible absorption spectra of PMB OMePhDPP (first scan) and after the oxidation cycle (final scan). Spectra were recorded in CH_2Cl_2 containing [n-Bu_4N][PF_6] (0.2 M) as the supporting electrolyte at 273 K.

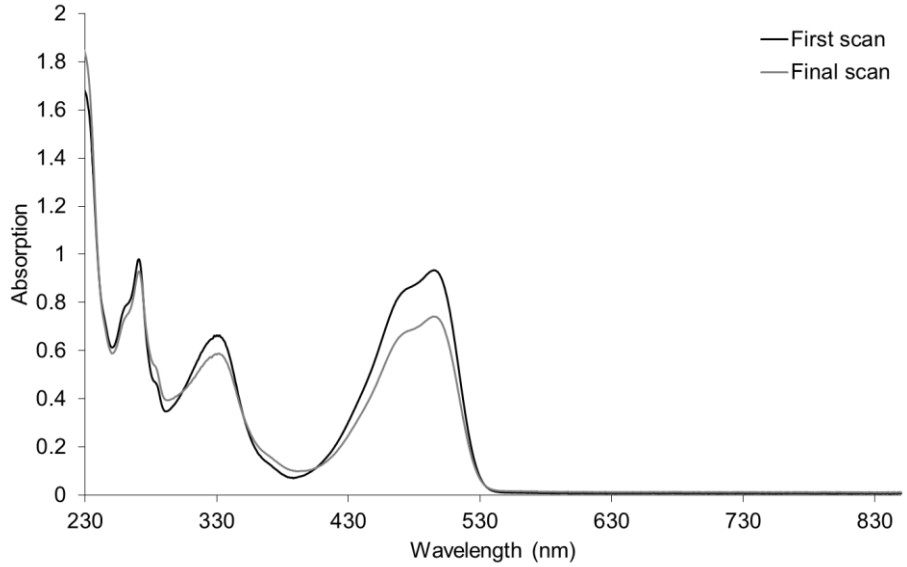

Figure SI7. UV-visible absorption spectra of PMB OMePhDPP (first scan) and after the reduction cycle (final scan). Spectra were recorded in CH_2Cl_2 containing [n-Bu_4N][PF_6] (0.2 M) as the supporting electrolyte at 273 K.

4. Theoretical calculations

All DFT calculations were performed using the Gaussian 09 software package.[SI1] Both the geometry optimisations and time-dependent excited state calculations were performed using the B3LYP exchange-correlation functional and the 6-31G (d) basis set. [SI2] Stationary points were characterised by normal mode vibrational frequency calculations. In all cases, the vibrational modes associated with the optimised structures did not exhibit imaginary frequencies, indicating that they represent minima on the potential energy surface.

Computationally determined molecular energy levels for methyl equivalent of Hex OMeDPP and Hex ThPhDPP:

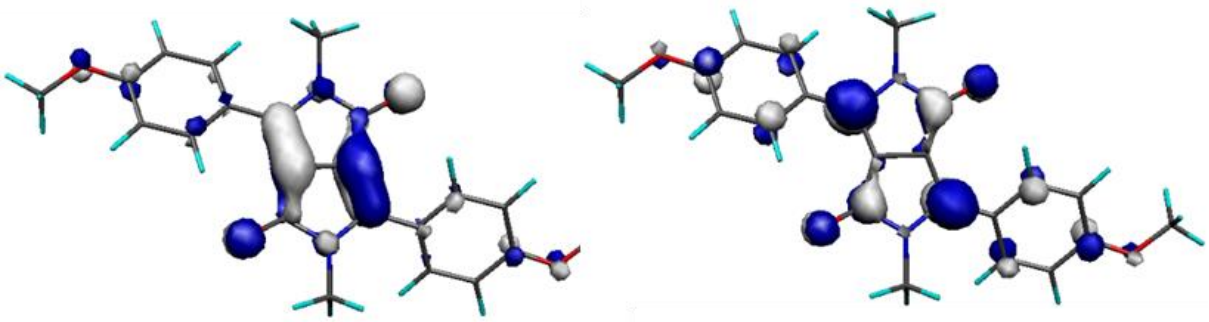

HOMO = -0.17676 (Hartrees) LUMO = -0.07754 (Hartrees)

HOMO and LUMO molecular orbitals for *N*-methyl OMePhDPP calculated by DFT as a model for long chain alkyl derivatives including Hex OMePhDPP.

Computationally determined molecular energy levels for Hex ThPhDPP

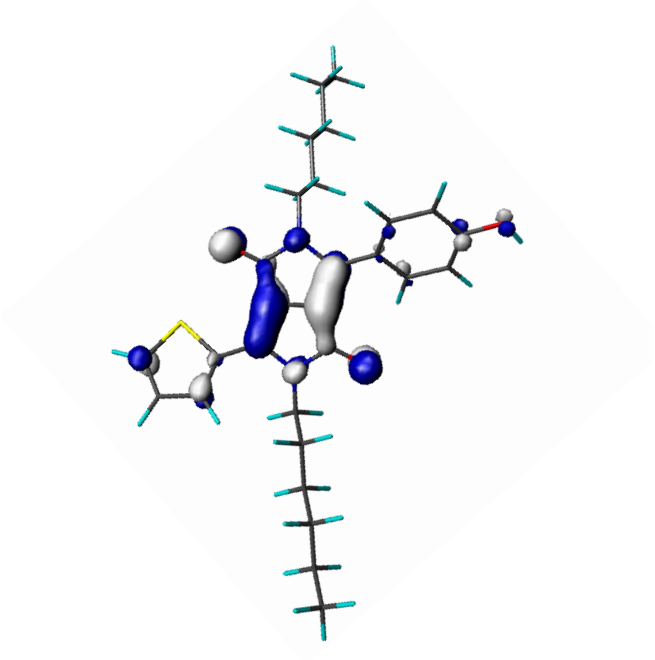

HOMO = -0.18125 (Hartrees)

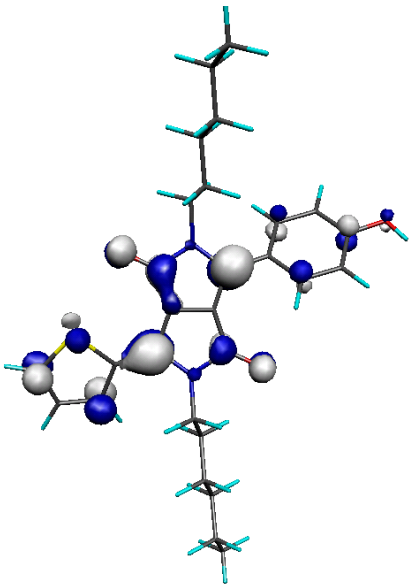

LUMO = -0.0832 (Hartrees)

5. Crystallographic data

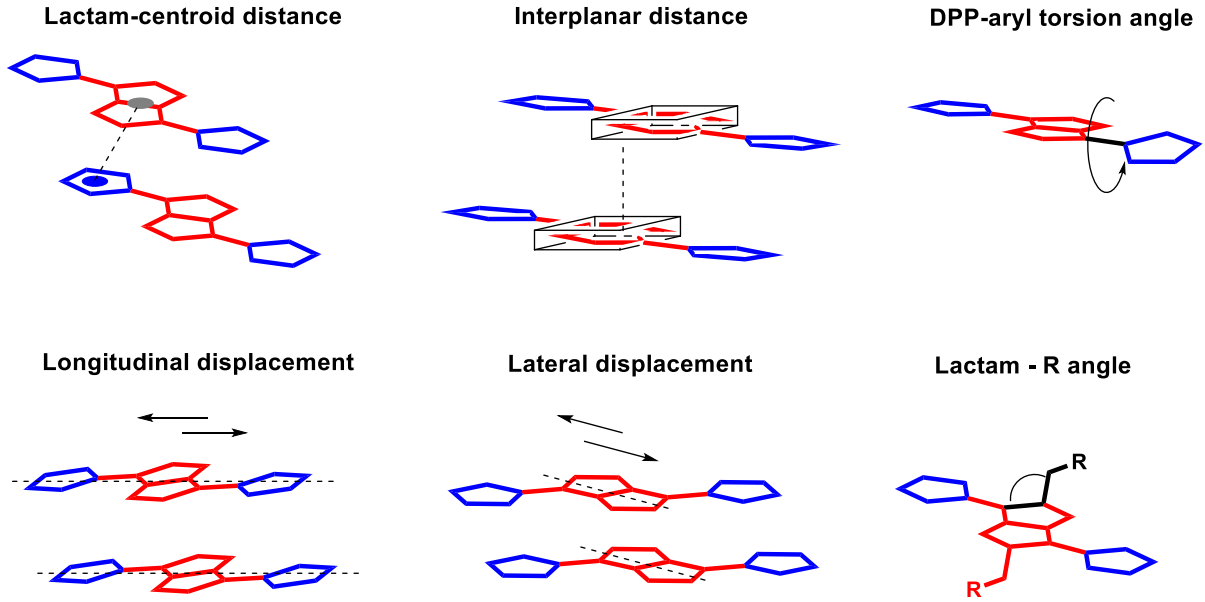

Figure SI8. Methods used to measure lactam-centroid distance, interplanar distance, longitudinal and lateral displacement, DPP- aryl angle and lactam – alkyl chain (R) angle.

Example calculation of aryl- lactam centroid distance

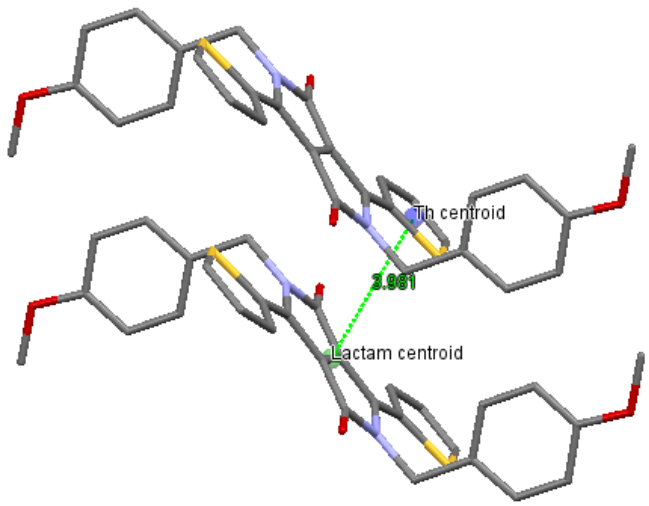

Example calculation of interplanar distance

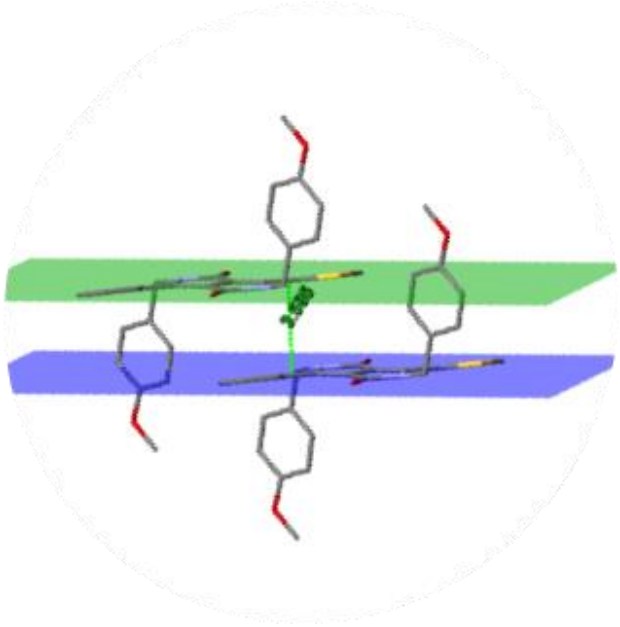

Example calculation of DPP- Aryl angle

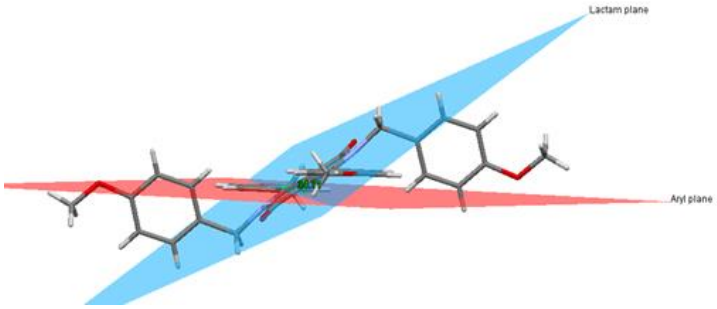

Example calculation of Lactam- [Clactam – N – C(R) angle

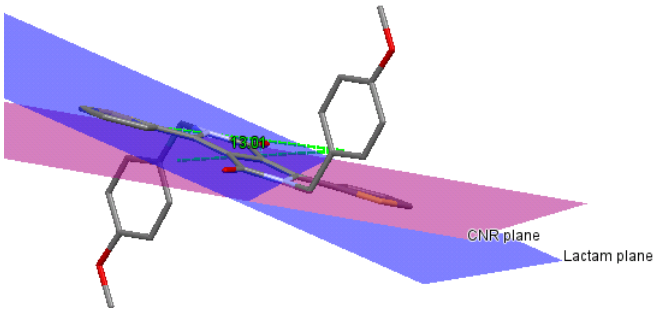

Stacking arrangement of 4MB ThDPP

Stacking arrangement of 4MB OMePhDPP

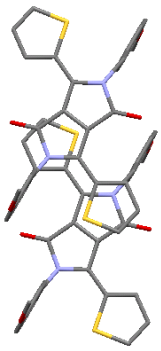

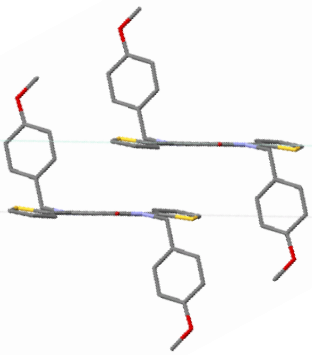

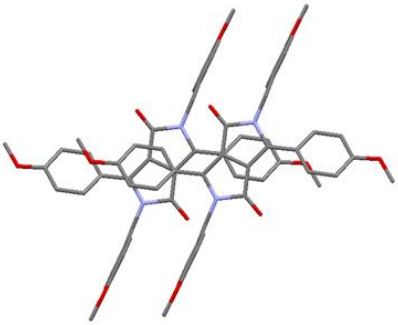

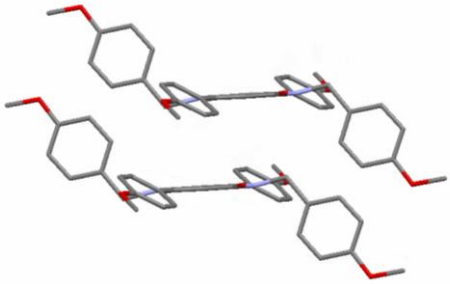

Stacking arrangement of 4MB ThPhDPP

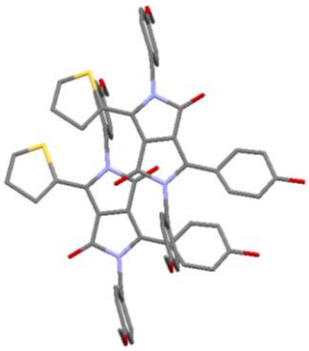

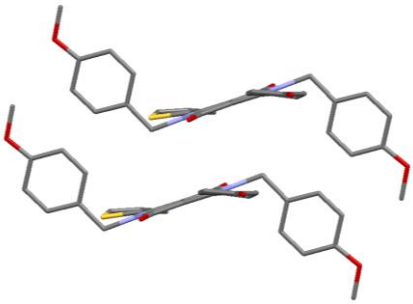

6. Solution state absorption and emission data for *n*- hexyl derivatives

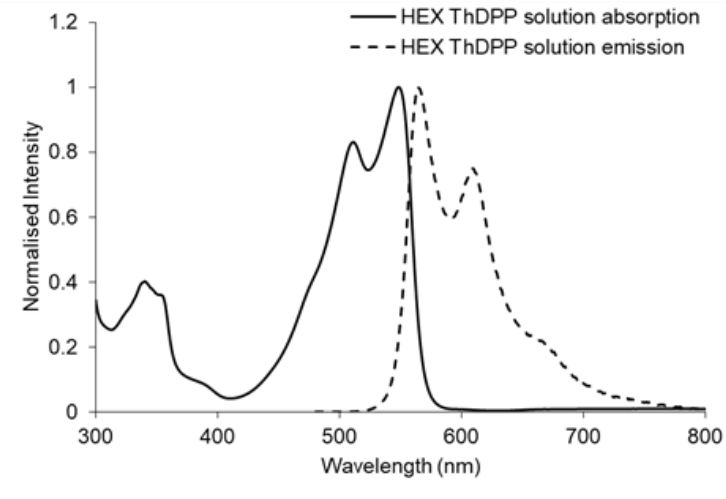

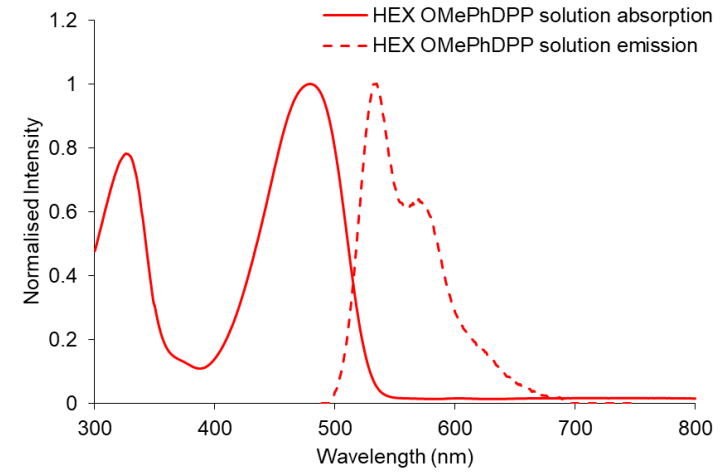

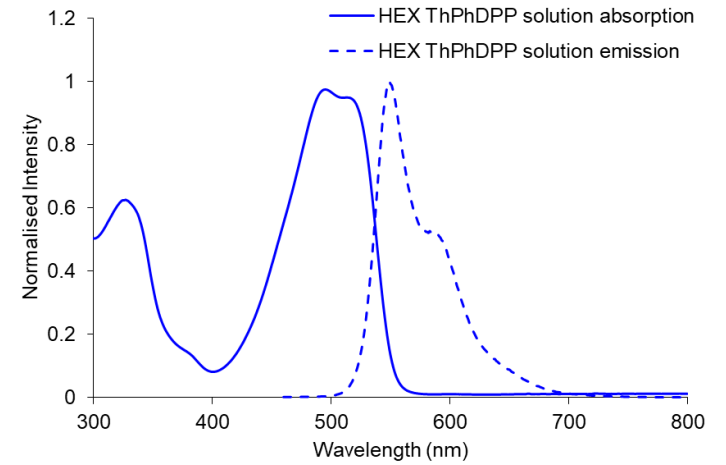

References

SI1. Gaussian 09, Revision D.01, M. J. Frisch, G. W. Trucks, H. B. Schlegel, G. E. Scuseria, M. A. Robb, J. R. Cheeseman, G. Scalmani, V. Barone, B. Mennucci, G. A. Petersson, H. Nakatsuji, M. Caricato, X. Li, H. P. Hratchian, A. F. Izmaylov, J. Bloino, G. Zheng, J. L. Sonnenberg, M. Hada, M. Ehara, K. Toyota, R. Fukuda, J. Hasegawa, M. Ishida, T. Nakajima, Y. Honda, O. Kitao, H. Nakai, T. Vreven, J. A. Montgomery, Jr., J. E. Peralta, F. Ogliaro, M. Bearpark, J. J. Heyd, E. Brothers, K. N. Kudin, V. N. Staroverov, T. Keith, R. Kobayashi, J. Normand, K. Raghavachari, A. Rendell, J. C. Burant, S. S. Iyengar, J. Tomasi, M. Cossi, N. Rega, J. M. Millam, M. Klene, J. E. Knox, J. B. Cross, V. Bakken, C. Adamo, J. Jaramillo, R. Gomperts, R. E. Stratmann, O. Yazyev, A. J. Austin, R. Cammi, C. Pomelli, J. W. Ochterski, R. L. Martin, K. Morokuma, V. G. Zakrzewski, G. A. Voth, P. Salvador, J. J. Dannenberg, S. Dapprich, A. D. Daniels, O. Farkas, J. B. Foresman, J. V. Ortiz, J. Cioslowski, and D. J. Fox, Gaussian, Inc., Wallingford CT, 2013.

SI2. (a) A. D. Becke, *Phys. Rev. A* **1988**, *38*, 3098. (b) A. D. Becke, *J. Chem. Phys.* **1993**, *98*, 5648. (c) C. Lee, W. Yang, R. G. *Parr, Phys. Rev. B* **1988**, *37*, 785.